VIRAL INFECTION

Quantitative phosphoproteomic analysis identifies the critical role of JNK1 in neuroinflammation induced by Japanese encephalitis virus

Jing Ye,[1,2,3,4] Hao Zhang,[1,2,4] Wen He,[1,2,4] Bibo Zhu,[1,2,4] Dengyuan Zhou,[1,2,4] Zheng Chen,[1,2,4] Usama Ashraf,[1,2,4] Yanming Wei,[1,2,4] Ziduo Liu,[1,3] Zhen F. Fu,[1,2,5] Huanchun Chen,[1,2,4] Shengbo Cao[1,2,4]*

Japanese encephalitis virus (JEV) is the leading cause of epidemic encephalitis worldwide. The pathogenesis of JEV is linked to a robust inflammatory response in the central nervous system (CNS). Glial cells are the resident immune cells in the CNS and represent critical effectors of CNS inflammation. To obtain a global overview of signaling events in glial cells during JEV infection, we conducted phosphoproteomics profiling of a JEV-infected glial cell line. We identified 1816 phosphopeptides, corresponding to 1264 proteins, that exhibited a change in phosphorylation status upon JEV infection. Bioinformatics analysis revealed that these proteins were predominantly related to transcription regulation, signal transduction, the cell cycle, and the cytoskeleton. Kinase substrate motif revealed that substrates for c-Jun N-terminal kinase 1 (JNK1) were the most overrepresented, along with evidence of increased AKT1 and protein kinase A (PKA) signaling. Pharmacological inhibition of JNK, AKT, or PKA reduced the inflammatory response of cultured glial cells infected with JEV, as did knockdown of JNK1 or its target JUN. JEV genomic RNA was sufficient to activate JNK1 signaling in cultured glial cells. Of potential clinical relevance, we showed that inhibition of JNK signaling significantly attenuated the production of inflammatory cytokines in the brain and reduced lethality in JEV-infected mice, thereby suggesting that JNK signaling is a potential therapeutic target for the management of Japanese encephalitis.

INTRODUCTION

Japanese encephalitis virus (JEV) is a neurotropic virus that causes severe encephalitic disease in human and animals. JE occurs predominantly in South, East, and Southeast Asia, as well as in Northern Australia, with more than 60,000 cases annually. The increase in cases may be the result of increased population density, deforestation, and expanding irrigation of agricultural areas (*1*, *2*). About 20 to 30% of clinical JE cases are fatal, and 30 to 50% of the survivors suffer from perpetual neurological sequelae. Even those JE patients with apparently good recovery have some persistent neurological deficits (*3*).

JEV is a mosquito-borne flavivirus belonging to the family *Flaviviridae*, which includes several other human pathogens, such as hepatitis C virus (HCV), West Nile virus (WNV), yellow fever virus, Zika virus, and dengue virus. JEV can cross the blood-brain barrier and reach the central nervous system (CNS), wherein viral replication leads to a robust inflammatory response and neuronal death (*4*, *5*). The pivotal factor in JEV-caused neuroinflammation is the rampant activation of glial cells (including microglia and astrocytes) (*6*, *7*), which release proinflammatory cytokines and chemokines, such as tumor necrosis factor–α (TNF-α), interleukin-1β (IL-1β), IL-6, chemokine (C-C motif) ligand 5 (CCL5, also called RANTES), and monocyte chemotactic protein 1 (MCP1, also called CCL2) (*8*, *9*). These proinflammatory cytokines promote massive leukocyte infiltration into the brain and induce death of both infected and noninfected (bystander) neurons (*4*, *10*, *11*). Analysis of cultured mouse microglia infected with JEV showed that signaling by the pattern recognition receptors TLR3 (Toll-like receptor 3) and RIG-I (retinoic acid–inducible gene-I) mediated the inflammatory response (*12*), and microRNA-15b (miR-15b) and miR-19b-3p promoted JEV-induced inflammation in cultured glial cells (*13*, *14*). However, further exploration for the molecular mechanism of JEV-induced neuroinflammation is still required.

Transcriptomic and proteomic approaches enable systems-level investigation of the complexity of virus-host interactions. Previously, we used RNA microarray technology to investigate messenger RNA (mRNA) profiles in spleen and brain tissues of mice infected with JEV, which showed the differential expression of 437 genes in spleen and 1119 genes in brain upon JEV infection (*15*). Proteomic analysis using stable isotope labeling with amino acids in cell culture (SILAC) identified changes in the abundance of 158 proteins in JEV-infected HeLa cells (*16*). These studies provide useful information for investigation of JEV pathogenesis and the development of therapeutic options.

Protein phosphorylation on serine (Ser), threonine (Thr), and tyrosine (Tyr) can regulate protein activity, influence protein structure, control subcellular distribution, and modulate interactions with other proteins, thereby regulating the signal transduction involved in cellular biological processes (*17*). High-throughput quantitative phosphoproteomics based on mass spectrometry (MS) is a powerful tool to analyze the protein phosphorylation profile (*18*, *19*). Because virus-induced cellular signaling cascades are involved in virus entry and replication and activation of the host antiviral response, a systematic and quantitative analysis of protein phosphorylation during virus infection provides crucial information about the molecular mechanisms of viral pathogenesis (*20*–*23*). To investigate the signaling events related to JEV-induced neuroinflammation, we performed label-free quantitative phosphoproteomics on a JEV-infected glial cell line, which identified >1200 proteins that exhibited a change in phosphorylation

[1]State Key Laboratory of Agricultural Microbiology, Huazhong Agricultural University, Wuhan, Hubei 430070, PR China. [2]Laboratory of Animal Virology, College of Veterinary Medicine, Huazhong Agricultural University, Wuhan, Hubei 430070, PR China. [3]College of Life Science and Technology, Huazhong Agricultural University, Wuhan, Hubei 430070, PR China. [4]The Cooperative Innovation Center for Sustainable Pig Production, Huazhong Agricultural University, Wuhan, Hubei 430070, PR China. [5]Department of Pathology, University of Georgia, Athens, GA 30602, USA. *Corresponding author. Email: sbcao@mail.hzau.edu.cn

state upon infection. Using bioinformatics tools, we analyzed the signaling pathways containing the infection-regulated phosphoproteins, predicted interacting networks of the phosphoproteins, and performed kinase substrate motif analysis to predict the kinases involved in infection-mediated regulation of the phosphoproteome. We found that substrates for c-Jun N-terminal kinase 1 (JNK1), also known as mitogen-activated protein kinase 8 (MAPK8), were significantly overrepresented in the phosphoproteins with increased phosphorylation in JEV-infected glial cells. Pharmacological inhibition of JNK1 signaling reduced the neuroinflammatory response and provided protection against acute encephalitis in a JEV-infected mouse model, which suggests the crucial role of JNK1 signaling in JEV pathogenesis and proposes a putative target for JE therapy.

RESULTS

Label-free, quantitative phosphoproteomics in JEV-infected U251 cells

To analyze the impact of JEV infection on protein phosphorylation in glial cells, we initially assessed the infectivity of JEV in the U251 cell line, which is a cell line derived from a human glioma and is positive for the glial marker glial fibrillary acidic protein (GFAP) (*24*) We infected the U251 cell line with the JEV P3 strain at multiplicities of infection (MOIs) of 1, 2, and 5 and assessed the viral infectivity by indirect immunofluorescence assay. JEV infected U251 cells in a dose-dependent manner (Fig. 1A). Using mock-infected or U251 cells infected with JEV at an MOI of 5, we used a phosphoproteomics strategy that combines phosphopeptide enrichment by TiO_2 and label-free quantification based on liquid chromatography coupled to tandem mass spectrometry (LC-MS/MS). We selected 12 hours because JEV begins to induce the massive expression of inflammatory cytokines in U251 cells by 12 hours after infection (fig. S1). We identified 1816 phosphopeptides, corresponding to 1264 phosphoproteins, in JEV-infected cells (table S1). The ratios (JEV-infected cells versus mock-infected cells) of phosphopeptides obtained from the two replicate experiments showed a strong positive correlation (r = 0.75) for two independent biological replicates (Fig. 1B). Most proteins were singly phosphorylated, and the phosphorylation events were biased toward Ser residues (Fig. 1C). Compared with mock-infected cells, a total of 872 phosphopeptides, corresponding to 604 proteins, were differentially regulated in JEV-infected cells, with 576 peptides increasing in phosphorylation (up-regulated phosphopeptides) (>2-fold) and 296

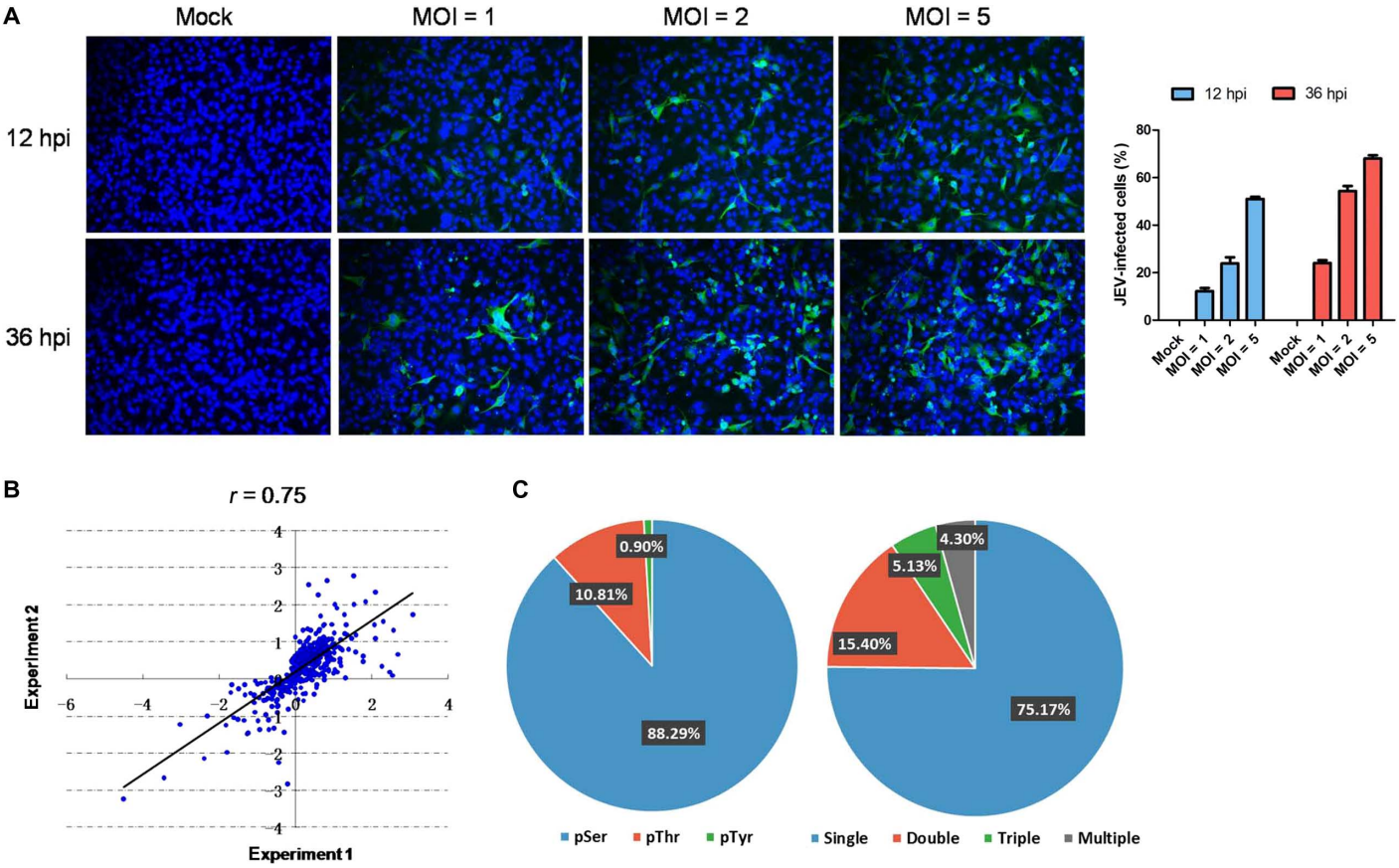

Fig. 1. Phosphoproteomic analysis of JEV-infected U251 cells. (**A**) Immunofluorescence staining of the viral protein NS5 in JEV-infected U251 cells. U251 cells were either mock-infected or infected with JEV at MOIs of 1, 2, and 5. Cells were fixed at 12 or 36 hours post-infection (hpi) and NS5 was detected by indirect immunofluorescence (green). Nuclei are shown by 4′,6-diamidino-2-phenylindole (DAPI) (blue) staining. The images of the cells were acquired with a fluorescence microscope (Zeiss) with 20× magnification. The graph shows the percentage of infected cells at the indicated conditions. (**B**) Reproducibility of the phosphoproteomic data. The reproducibility between two biological replicates was determined by calculating the Pearson correlation coefficient (r) on a density scatterplot of $\log_2$-transformed phosphopeptide ratios of the JEV-infected cells versus the mock-infected cells. (**C**) Left: Distribution of serine (pSer), threonine (pThr), and tyrosine (pTyr) phosphorylation based on detected phosphosites. Right: Distribution of single, double, triple, and greater than triple (multiple) phosphosites based on detected phosphopeptides.

peptides decreasing in phosphorylation (down-regulated phosphopeptides) (<0.5-fold) (table S2), indicating that JEV has a substantial impact on host protein phosphorylation.

Cellular processes affected by JEV infection

To gain insight into the biological functions of proteins in the phosphoproteome regulated by JEV infection, we associated Gene Ontology (GO) terms to the proteins with the functional annotation tool of the Database for Annotation, Visualization, and Integrated Discovery (DAVID, version 6.7; http://david.abcc.ncifcrf.gov/). The results showed that proteins were involved in diverse cellular functions with a specific enrichment in proteins related to transcription regulation, signaling cascade, RNA processing, the cell cycle, the cytoskeleton, and intracellular transport (Fig. 2A, Biological process, and tables S3 and S4). To help identify specific signal transduction pathways affected by JEV infection, we analyzed the data using the Kyoto Encyclopedia of Genes and Genomes (KEGG) pathways database (tables S3 and S4) (*25*). The key cellular pathways for up-regulated phosphoproteins included cancer, endocytosis, phagocytosis, and cytotoxicity signaling, whereas the most notable cellular pathways for down-regulated phosphoproteins are tight and adherens junction signaling, suggesting that inflammation-related signaling pathways were activated during JEV infection (Fig. 2A, KEGG pathway). Pathway analysis also indicated increased activity of several kinase-mediated signaling pathways in JEV-infected cells, including the serine/threonine-specific protein kinase (AKT), MAPK, protein kinase C (PKC), protein kinase A (PKA), and p21-activated protein kinase (PAK) pathways (Fig. 2B).

We used Ingenuity Pathway Analysis (IPA, versions 1.0 to 4.0) to assemble a protein network based on the JEV-regulated phosphoproteins with at least one connection identified by IPA (fig. S2 and table S5). This analysis showed a complex network with several distinct functional modules. Proteins, such as AKT1, MAPK1 [also known as extracellular signal–regulated protein kinase 1 (ERK1)], MAPK3 (also known as ERK2), JUN (also known as c-Jun), tumor protein 53 (TP53, also known as p53), PKA catalytic subunit α (PRKACA), and PKCα, were highly connected with other proteins. In addition, the phosphatidylinositol 3-kinase (PI3K) complex, the nuclear factor κB (NF-κB) complex, and the JNK group were predicted to play central

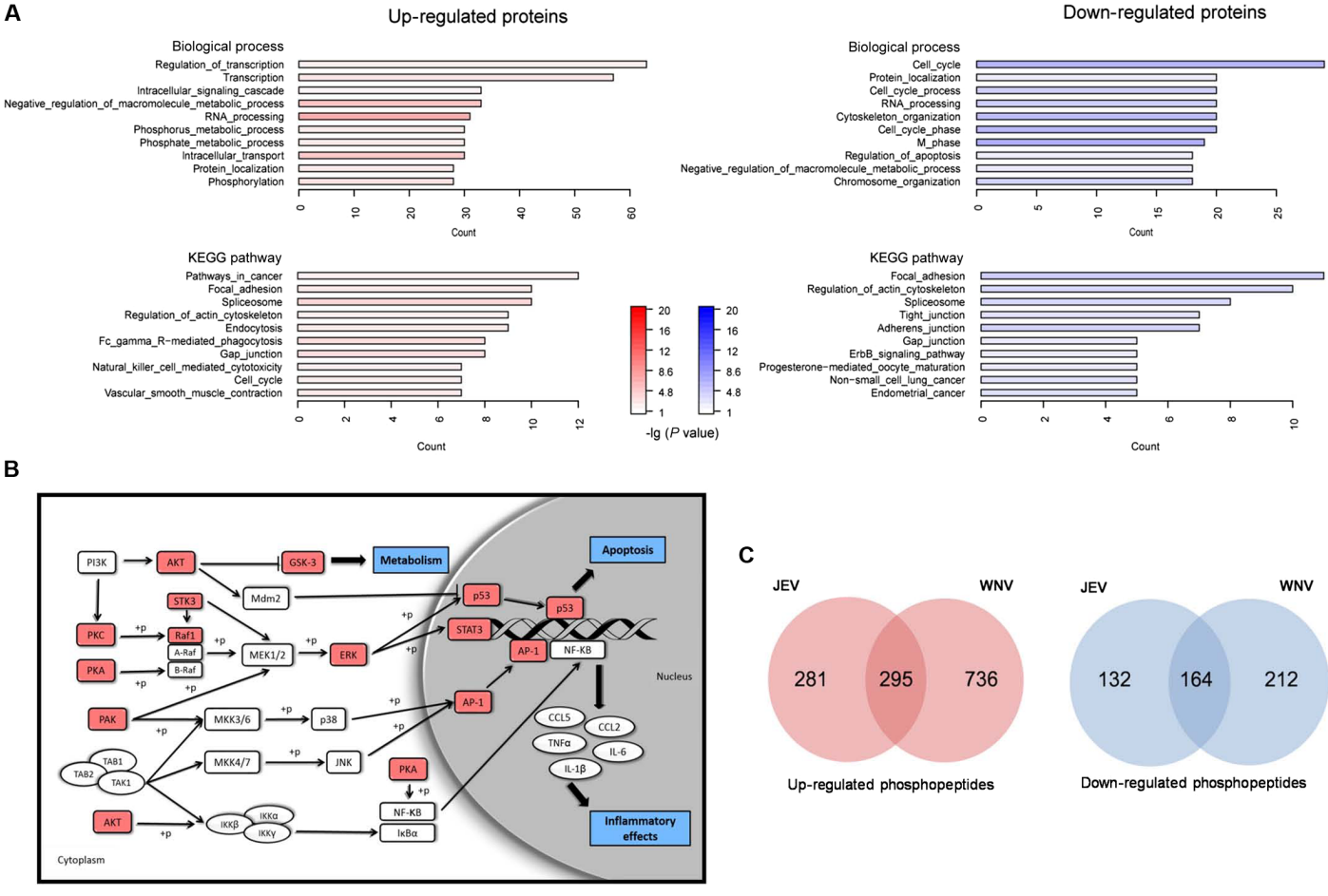

Fig. 2. Cellular processes affected by JEV infection. (**A**) GO analysis of proteins with altered phosphorylation after JEV infection performed with DAVID (GO term BP FAT, $P < 0.05$). All proteins containing at least one phosphopeptide with a minimum twofold change were considered for analysis. (**B**) Diagram of the signaling pathways that converge on up-regulated and down-regulated phosphoproteins identified by phosphoproteomics. Proteins from the phosphoproteome of JEV-infected cells are shown in red. Other proteins were not detected in the phosphoproteomics study. GSK-3, glycogen synthase kinase 3; Mdm2, mouse double minute 2; STK3, serine/threonine kinase 3; STAT3, signal transducer and activator of transcription 3; AP-1, activator protein 1; MKK3/6 and MKK4/7, MAPK kinase 3/6 and kinase 4/7; IKK, inhibitor of κB (IκB) kinase. (**C**) Venn diagram showing the overlap of up-regulated (left panel) and down-regulated (right panel) phosphopeptides after JEV and WNV infection.

roles in the interaction network. The network included kinases and other catalytically active enzymes, transcription and translation factors, transporters, and cytokines, consistent with JEV infection of glial cells resulting in the stimulation of signal transduction pathways that regulate gene expression and protein translation and the release of cytokines.

Because JEV and WNV are related viruses, we compared the data from the JEV-infected U251 cells to a phosphoproteome data set from WNV-infected U251 cells that was obtained with the same quantitative phosphoproteomics method (*23*). This analysis showed ~20% overlap in the up-regulated and down-regulated phosphopeptides (Fig. 2C), suggesting that cells infected by JEV or WNV exhibit similar changes in phosphorylation events. Proteins involved in gene regulation, signal transduction, and the cytoskeleton exhibited similar phosphorylation changes in cells infected with either virus (table S6). These results indicated that common molecular processes are triggered by infection of glial cells by JEV or WNV.

Identification of overrepresented kinase phosphorylation motifs

The phosphorylation of many kinase substrates is influenced by the amino acids that immediately surround the phosphorylation site; this sequence of amino acids is referred to as the kinase phosphorylation motif. Although many kinases are activated by a change in phosphorylation status and thus the effect of JEV infection on their activity could be predicted from the phosphoproteomic data, we also used kinase phosphorylation motif analysis to identify additional kinases that may be activated by JEV infection and to predict which kinases may be particularly important to the response to infection on the basis of the overrepresentation of their kinase phosphorylation motifs in the up-regulated phosphoproteome. We analyzed the amino acid residues surrounding each JEV-responsive phosphorylation site using the Group-based Prediction System (GPS) and the motif extractor (Motif-x) tool. The GPS uses a hierarchical algorithm to rank the likelihood that a particular kinase or kinase family phosphorylates a given phosphorylation site, whereas Motif-x measures the overrepresentation of amino acid sequence patterns, thereby providing a list of potential kinase substrate motifs. According to Fisher's exact test, substrates for JNK1 (MAPK8) were significantly overrepresented in the up-regulated phosphoproteins, whereas substrates for casein kinase II (CK2) were overrepresented in down-regulated phosphoproteins (table S7). JNK1 is a member of the MAPK family and phosphorylates a number of transcription factors, primarily components of the AP-1 transcriptional complex, including JUN, JDP2, and ATF2 (*26*, *27*). Of these, we identified JUN as exhibiting increased phosphorylation upon JEV infection.

To identify the phosphorylation motifs overrepresented in the JEV-regulated phosphoproteome, we applied the Motif-x algorithm (*28*) to all up-regulated phosphopeptides, which resulted in the identification of three serine-based phosphorylation motif sequences SP, SDXE, and SSP (Fig. 3 and table S8). To predict the putative kinases of these motifs, we compared these motifs to those of all known substrates of 107 kinase families (*29*). SP is a motif found in many JNK, ERK, GSK-3, and cyclin-dependent kinase substrates, whereas SDXE is one of many motifs that is phosphorylated by CK2. The motif analysis and the overrepresentation of phosphoproteins predicted to be substrates of JNK1 support an increase in JNK1 activity during JEV infection. ERK2 is another kinase that recognizes substrates with the SP motif. We found an increase in the phosphorylated form of ERK2

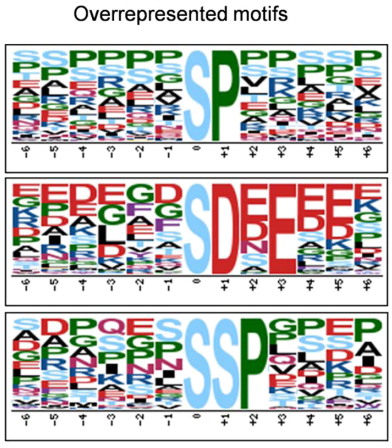

Fig. 3. Top-ranked three putative kinase substrate motifs within up-regulated JEV-responsive phosphorylation sites. The amino acid position weighted matrix, centered on phosphorylated serine (position 0), is shown for each top-scoring motif.

that corresponds to the activated form of this MAPK in the JEV-infected cells, which is consistent with a previous study (*30*, *31*); therefore, ERK2 may also contribute to the phosphorylation of proteins with the SP motif.

Involvement of AKT1, PRKACA, and JNK1 signaling pathways in the JEV-induced inflammatory response of glial cells

To corroborate the changes in protein phosphorylation levels induced by JEV infection, we selected the proteins AKT1, PRKACA, and TP53 on the basis of their high connectivity with other proteins (figs. S2 and S3) and their possible involvement in inflammatory signaling pathways. In addition, we validated the changes in phosphorylation status of JNK1, which was identified as the most overrepresented protein kinase in JEV-infected cells, and its well-known substrate JUN (c-Jun). We performed a time course of infection and assessed site-specific phosphorylation in JEV-infected U251 cells and in the mouse microglial cell line BV-2 by Western blotting. NS5 served as a viral marker of infection. Consistent with the MS data obtained from U251 cells at 12 hours after infection, phosphorylation of AKT1 at Ser^{124}, JNK1 at Thr^{183} and Tyr^{185}, and c-Jun at Ser^{63} apparently increased in the infected cells, as did the phosphorylation of PRKACA at Thr^{198} (Fig. 4A). Each of these phosphorylation events is associated with increased kinase activity (*32*–*35*). Also consistent with the MS data, TP53 exhibited reduced phosphorylation at Ser^{392}; a reduction in phosphorylation at this site is associated with increased TP53 transcriptional activity (*36*). Infection did not appear to alter the abundance of the analyzed proteins. Analysis of infected BV-2 and mouse brain tissue from infected and mock-infected mice revealed similar trends for the phosphorylated proteins, except for TP53, which did not appear to have any change in phosphorylation in the mouse brain.

Because the phosphorylation levels of AKT1, PRKACA, TP53, and JNK1 changed in response to JEV infection, we investigated their roles in JEV-induced inflammation. We compared cytokine release from infected or mock-infected U251 and BV-2 cells that had been pre-exposed to specific inhibitors of AKT (API-59CJ-OMe), PKA (H89), or JNK (SP600125) or an activator of TP53 (JNJ-26854165). Release of the inflammatory cytokines TNF-α, IL-1β, IL-6, and CCL2 [measured in the supernatant by enzyme-linked immunosorbent assay (ELISA) at 24 and 36 hours after infection] increased in response to JEV infection

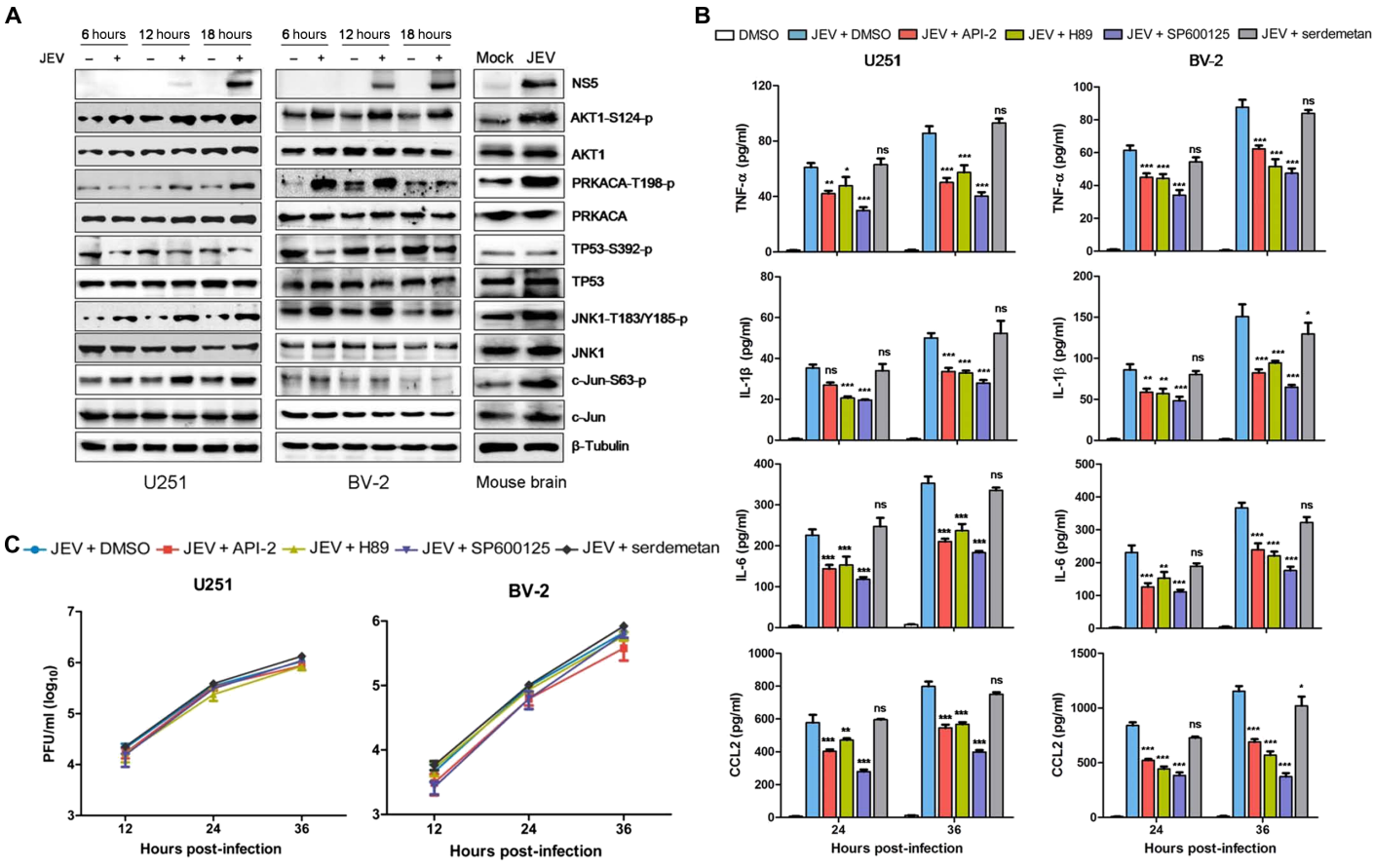

Fig. 4. Validation of the roles of AKT1, PRKACA, TP53, and JNK1 in JEV-induced inflammation. (**A**) Immunoblot analysis of AKT1, PRKACA, TP53, and JNK1 phosphorylation in cells and mouse brain with JEV infection. U251 and BV-2 cells were infected with JEV at an MOI of 5 and cells were harvested at 6, 12, and 18 hours after infection. BALB/c mice were inoculated intracranially with 20 ml of phosphate-buffered saline (PBS) or 50 plaque-forming units (PFU) of JEV in 20 ml of PBS, and the brain tissues were collected at 5 days after infection. The cell extracts from U251 and BV-2 cells and mouse brain homogenate were subjected to Western blot analysis with antibodies recognizing the indicated proteins. Data are representative of three independent experiments. (**B**) U251 and BV-2 cells were treated with dimethyl sulfoxide (DMSO), 12 μM API-59CJ-OMe (AKT inhibitor), 30 μM H89 (PKA inhibitor), 5 μM SP600125 (JNK inhibitor), or 10 μM JNJ-26854165 (TP53 activator). After incubation for 6 hours, DMSO-treated cells were mock-infected or infected with JEV at an MOI of 5, and the inhibitor-treated cells were infected with JEV. The supernatants were collected 24 hours after infection and subjected to ELISA to measure the concentration of indicated inflammatory cytokines. Data are expressed as means ± SEM from three independent experiments. $^{*}P < 0.05$, $^{**}P < 0.01$, $^{***}P < 0.001$, two-way analysis of variance (ANOVA) with subsequent Bonferroni post test; ns, not significant. (**C**) U251 and BV-2 cells treated with DMSO or indicated compound were infected with JEV at an MOI of 1. Cells were collected at 12, 24, and 36 hours after infection, and viral titers were determined by plaque assay. API-2, Triciribine (an AKT inhibitor).

in both cell lines (Fig. 4B). However, inhibition of AKT, PKA, or JNK, but not addition of the activator for TP53, significantly reduced the amounts of these cytokines produced by JEV-infected U251 and BV-2 cells at both 24 and 36 hours after infection, indicating that AKT, PKA, and JNK signaling pathways are involved in the JEV-induced inflammatory response in glial cells. To determine whether the activity of these proteins affected JEV replication, we monitored the viral titers in inhibitor-treated or untreated cells. Viral replication was unaffected by inhibition of these signaling pathways, indicating that targeting the inflammatory response may not prevent JEV replication in the glial cells (Fig. 4C).

Promotion of the JEV-induced inflammatory response by glial cells by the JNK1-AP-1 signaling pathway

The JNK pathway is a key inflammatory pathway, and JNK1 signaling induces the expression of genes encoding matrix metalloproteinases (MMPs), which are implicated in neuroinflammatory diseases by contributing to (i) the increased permeability of the blood-brain and blood-nerve barriers, (ii) invasion of neural tissue by blood-derived immune cells, and (iii) direct cellular damage (*37*–*40*). Preexposing U251 and BV-2 cells to the JNK-specific inhibitor SP600125 produced a dose-dependent inhibition of JEV infection–induced JUN (a component of the AP-1 transcriptional regulatory complex) and JNK1 phosphorylation at activating sites (Fig. 5A), suggesting that JNK1 can mediate the activation of AP-1 during JEV infection. SP600125 also reduced the amount of MMP3 and MMP9 detected in the culture medium of JEV-infected cells (Fig. 5B), consistent with JNK1 signaling stimulating the expression of *MMP3* and *MMP9* during JEV infection. To further confirm the effect of JNK1 activation on JEV-induced inflammation, we overexpressed JNK1 or knocked down JNK1 or JUN by small interfering RNA (siRNA) in U251 cells (Fig. 5C), infected the cells with JEV, and monitored the production of inflammatory cytokines and MMPs (Fig. 5D). As expected, knockdown of JNK1 reduced the levels of inflammatory cytokines and MMPs elicited by JEV infection, whereas overexpression of JNK1 had an opposite effect (Fig. 5C). JUN knockdown reduced the production of

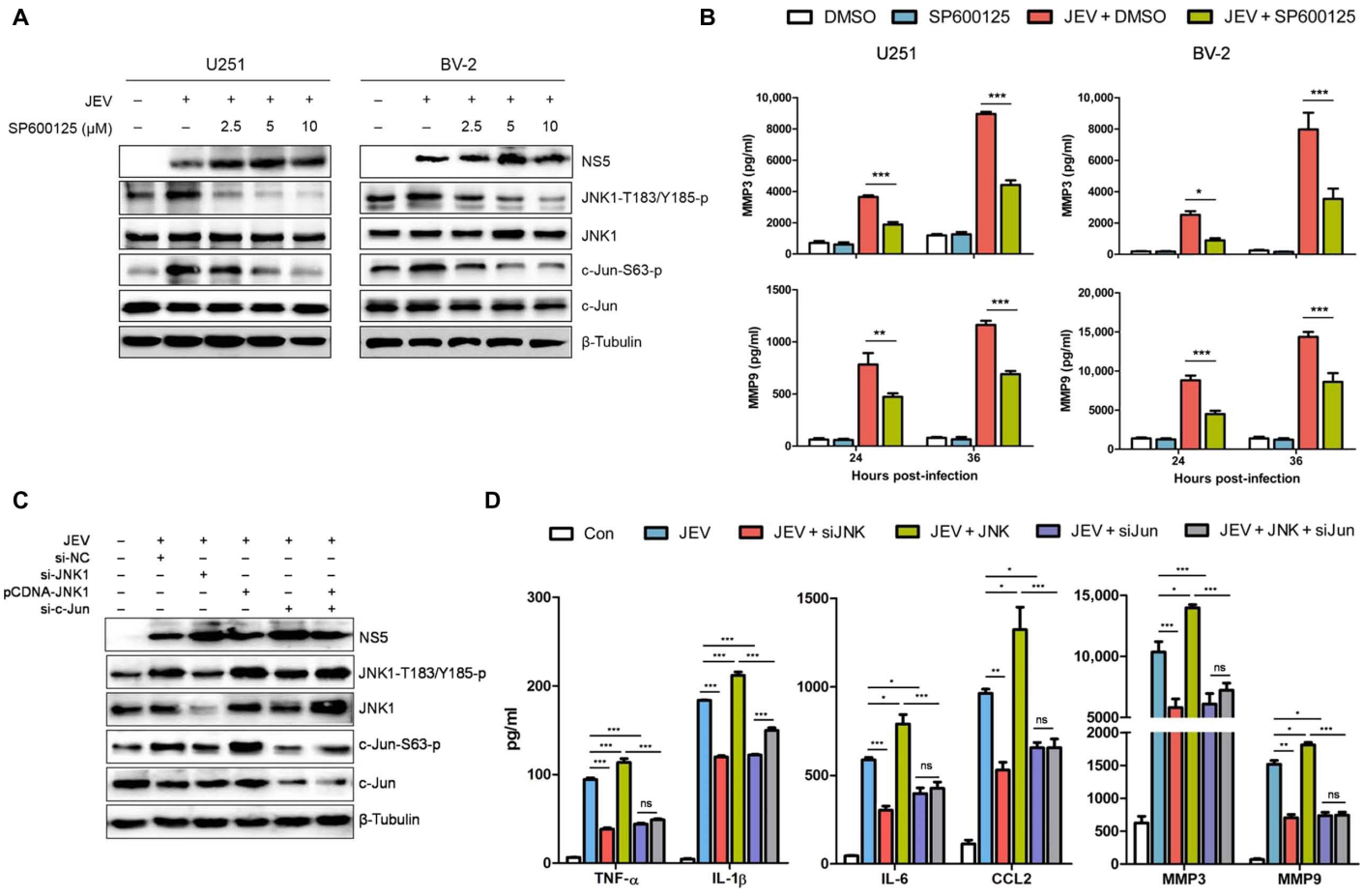

Fig. 5. JNK1-AP-1 signaling pathway mediates JEV-induced inflammation. (**A**) Effect of JNK inhibitor on JNK1-AP-1 signaling. U251 and BV-2 cells were left treated with DMSO or increasing amounts (2.5, 5, or 10 μM) of the JNK inhibitor (SP600125). After incubation for 6 hours, DMSO-treated cells were mock-infected or infected with JEV at an MOI of 5, and the inhibitor-treated cells were infected with JEV. Twelve hours after infection, phosphorylation of JNK1 and c-Jun was analyzed by Western blotting. Data are representative of three independent experiments. (**B**) U251 and BV-2 cells were treated with DMSO or 5 μM SP600125 followed by mock infection or JEV infection for 24 hours. The supernatants were collected and subjected to ELISA to measure the concentration of MMP3 and MMP9. (**C** and **D**) U251 cells were left untreated or transfected with siRNA for negative control (si-NC), siRNA for JNK1 (si-JNK1), expression plasmid for JNK1 (pcDNA-JNK1), siRNA for c-Jun (si-c-Jun), or pcDNA-JNK1 and si-c-Jun. After 24 hours, transfected cells were infected with JEV at an MOI of 5. Twenty-four hours after infection, cell extracts were subjected to Western blotting to detect the indicated proteins (C). Concentrations of cytokines in cell supernatants were determined by ELISA assay (D). Data were expressed as means ± SEM from three independent experiments. *$P < 0.05$, **$P < 0.01$, ***$P < 0.001$, two-way ANOVA with subsequent Bonferroni post test.

inflammatory cytokines and MMPs in JEV-infected cells both in the presence and in the absence of overexpressed JNK1, consistent with JUN functioning downstream of JNK in the inflammatory response to JEV infection.

Activation of JNK1 signaling by JEV genomic RNA

To investigate the mechanism by which JEV elicits the activation of JNK1 signaling pathway, we exposed U251 cells to JEV or UV-irradiated, inactivated JEV and assessed JNK1 phosphorylation by Western blotting. UV-irradiated, inactivated JEV did not accumulate in the cells (Fig. 6A, NS5), nor did the inactivated virus affect JNK1 phosphorylation at Thr^{183} or Tyr^{185} (Fig. 6A, JNK1-T183/Y185-p), suggesting that active infectious virus is required to stimulate JNK1. To further probe which viral component contributes to the activation of JNK1 signaling pathway, we individually transfected U251 cells with plasmids expressing each of the JEV nonstructural proteins and measured the JNK1 phosphorylation status. None of these JEV proteins individually stimulated JNK1 phosphorylation (Fig. 6B). In contrast, introduction of viral genomic RNA, which was extracted from cells infected with increasing MOI of JEV, into U251 cells resulted in an apparent dose-dependent increase in JNK1 phosphorylation, a response that did not occur with RNA extracted from mock-infected cells (Fig. 6C). To exclude the possibility that cellular mRNA, rather than viral RNA, induced JNK1 phosphorylation, we transfected in vitro transcribed JEV replicon RNA into U251 cells. This JEV replicon RNA elicited JNK1 phosphorylation within 6 hours of transfection at a time when there was little detectable viral protein (Fig. 6D), indicating that JEV genomic RNA participates in JNK1 activation.

Reduction of viral load and prevention of JEV-induced lethality by a JNK1 inhibitor

To assess the role of JNK1 signaling in JEV-induced neuroinflammation and lethality in vivo, we used a mouse model of JEV infection and tested the effect of the JNK inhibitor SP600125. We administered SP600125 intravenously into mice on days 3 and 4 after JEV infection

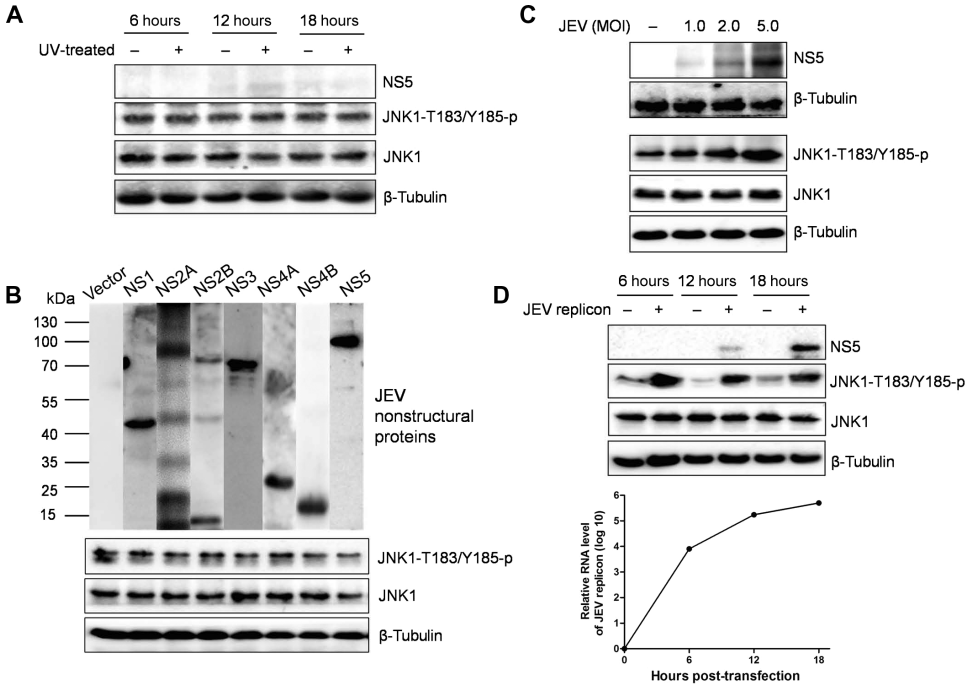

Fig. 6. JEV genomic RNA contributes to the activation of JNK1 signaling. (**A**) U251 cells were incubated with UV-irradiated inactive JEV for the indicated times. JNK1 phosphorylation was analyzed by Western blotting. (**B**) U251 cells were transfected with empty vector or plasmid encoding each of the JEV nonstructural proteins as indicated for 24 hours. JEV proteins and JNK1 phosphorylation were detected by Western blotting. (**C**) U251 cells were mock-infected or infected with JEV at an MOI of 1, 2 or 5 for 36 hours. JEV protein NS5 was analyzed by Western blotting. Whole cellular RNA was extracted and transfected into U251 cells for 12 hours. JNK1 phosphorylation was detected by Western blotting. (**D**) Plasmid containing JEV replicon and empty vector was in vitro transcribed. The transcribed products were transfected into U251 cells. After incubation for indicated 6, 12, or 18 hours, JNK1 phosphorylation was determined by Western blotting, and the RNA abundance of the JEV replicon was analyzed by quantitative real-time polymerase chain reaction (qRT-PCR). All data are representative of three independent experiments.

(Fig. 7A) and killed the mice and collected brain tissues on days 5 and 23 after infection. We chose these two times because the mice started to develop typical symptoms of encephalitis on day 5 after infection and most surviving mice were recovered on day 23 after infection.

To determine the viral load in the mouse brain, we measured the viral titers by plaque assay. Brain homogenates prepared on day 5 after infection from SP600125-treated and JEV-infected mice showed a significant reduction in viral titers compared with that from untreated infected mice (Fig. 7B). We assessed survival rate over the 23 days. All of the mock-infected mice or mock-infected mice that received SP600125 survived until the end of the experiment at 23 days when they were killed (Fig. 7C). In contrast, all mice in the JEV infection group that did not receive any treatment died within 7 days after infection (Fig. 7C). Forty percent of the JEV-infected mice that received SP600125 survived and exhibited improved behavior compared with their behavior at 5 days after infection, suggesting that administration of the JNK inhibitor can protect against JEV-induced mortality and possibly inflammatory damage.

Attenuation of neuroinflammation by JNK1 inhibitor treatment of a JEV-infected mouse model

To determine whether survival and the beneficial effects of SP600125 correlated with reduced activation of inflammatory signaling by JNK1, we measured phosphorylation of JNK1 and JUN in the brains of JEV-infected mice at 5 days after infection. Although the effect of SP600125 treatment on JNK1 phosphorylation was ambiguous, JUN phosphorylation appeared reduced compared with that in the JEV-infected and untreated mouse brains (Fig. 8A), consistent with SP600125 inhibiting JNK1 signaling in the brain. Consistent with the reduction in viral load (Fig. 7B), we also observed apparently less viral protein NS5 in the brains of JEV-infected mice receiving SP600125 (Fig. 8A).

We also assessed the abundance of inflammatory cytokines (TNF-α, IL-1β, IL-6, and CCL-2) in the mouse brain. Five days after infection, viral infection triggered the release of large amounts of inflammatory cytokines, whereas SP600125 treatment significantly reduced cytokine concentrations in the mouse brain (Fig. 8B). Twenty-three days after infection, cytokine abundance in the recovered mice that had received SP600125 was decreased to the normal amount, indicating that SP600125 treatment reduced the production of inflammatory cytokines in the mouse brain during JEV infection.

Furthermore, analysis of histopathological changes in mouse brains by hematoxylin and eosin (H&E) staining of cerebrum showed that the mice that were not infected with JEV did not exhibit any histological alteration regardless of whether the mice had received SP600125 or not (Fig. 8C, top row). We detected meningitis and perivascular cuffing, which are indicators of severe encephalitis in JEV-infected mice at 5 days after infection, whereas these indicators of encephalitis were reduced in JEV-infected mice receiving SP600125 treatment (Fig. 8C). The surviving JEV-infected and SP600125-treated mice had normal histology in this part of the brain at 23 days after infection.

To determine the effect of SP600125 on JEV-triggered microgliosis and astrocytosis, we stained the brain sections with antibodies recognizing the microglia marker protein IBA-1 and the astrocyte marker protein GFAP. Brains of JEV-infected mice had many star-shaped, activated microglia at 5 days after infection, whereas SP600125 treatment reduced the appearance of these cells (Fig. 8C). Similarly, JEV-infected and SP600125-treated mice had fewer activated astrocytes compared with JEV-infected mice (Fig. 8C).

We also assessed neuronal cell death in brain tissue sections with the TUNEL (terminal deoxynucleotidyl transferase–mediated deoxyuridine triphosphate nick end labeling) assay. NeuN indicated neurons, and TUNEL indicated dying cells. The ratio of NeuN-positive and TUNEL-negative cells was increased by SP600125 treatment in JEV-infected mice on 5 dpi (Fig. 9). Thus, inhibiting the JNK pathway has the potential to prevent neuronal cell damage during JEV infection. These results and the survival data showed that inhibition of JNK signaling attenuated JEV-mediated neuroinflammation and may improve survival with reduced long-term neurological dysfunction.

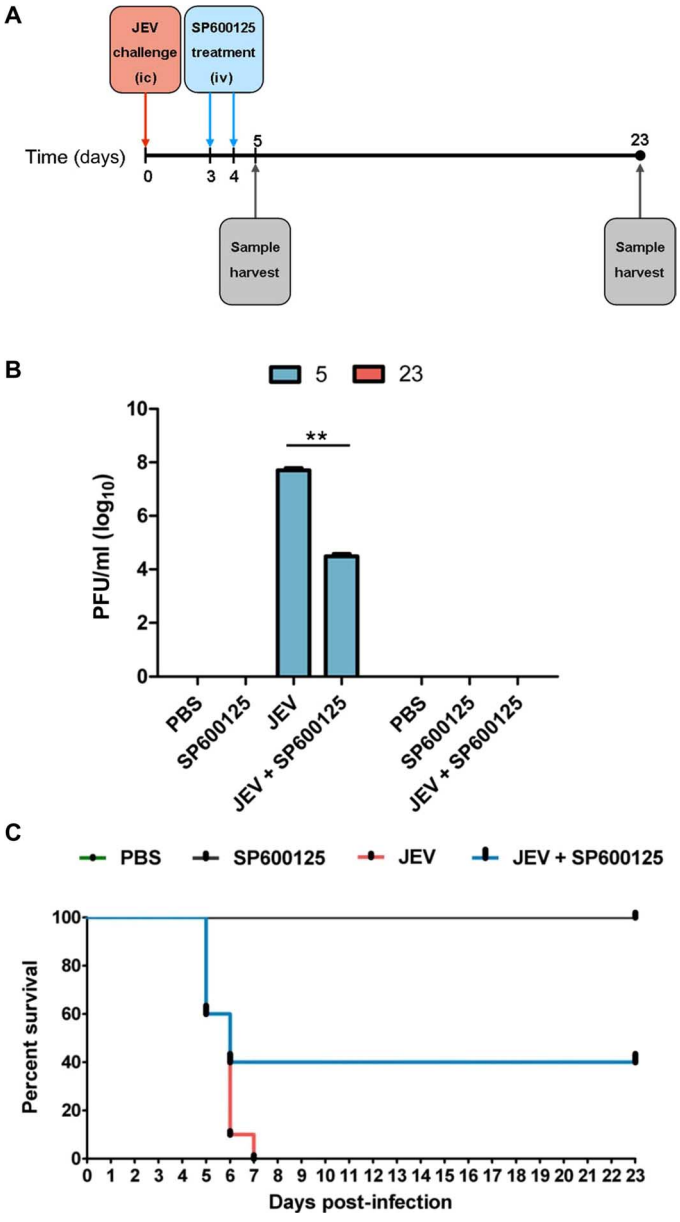

Fig. 7. JNK1 inhibitor treatment reduces viral load in the mouse brain and prevents lethality in JEV-infected mouse model. (**A**) Diagram of in vivo experiment model. Mice were inoculated intracranially (ic) with PBS or JEV (50 PFU per mice) followed by intravenous (iv) injection with DMSO or SP600125 (15 mg/kg) on days 3 and 4 after infection. Brain samples were collected on days 5 and 23 after infection. (**B**) Viral titers in the mouse brain on days 5 and 23 after JEV infection were determined by plaque assay. The viral titers are shown as $\log_{10}$ PFU/ml (n = 3 mice). $^{**}P < 0.001$, Student's t test. (**C**) Survival of mice in each group was monitored for 23 days after JEV inoculation. Data were collected and shown as Kaplan-Meier survival curves (n = 10 mice).

DISCUSSION

Uncontrolled inflammation in the CNS is the major cause of death during JEV infection. Understanding the molecular mechanisms and unveiling druggable protein targets that mediate JEV-mediated neuroinflammation are urgent and unmet needs for developing novel therapeutic methods for patients suffering from this infection. Furthermore, because this virus is in the same family as several other viruses (including Zika and WNV) that cause neurological pathology, understanding the inflammatory response to JEV may inform treatment strategies for those viruses as well.

Through phosphoproteome profiling of JEV-infected glial cells at a single time point after infection, we found more than 300 proteins that exhibited a significant change in phosphorylation status upon infection. We expect this number to be an underestimate of the JEV infection–regulated phosphoproteome because of experimental and technical limitations. Consistent with the pathology of microgliosis and astrocytosis, which appear as abnormal increases in cell number and shape changes (*11*), in JEV-infected brain, GO analysis and manual functional annotation of the phosphoproteome revealed the importance of the cell cycle and actin cytoskeleton during infection. Furthermore, phagocytosis and cytotoxicity signaling pathways were associated with JEV infection, which is consistent with the activation of inflammatory response induced by JEV infection.

Our pathway analysis identified enhanced activity of multiple kinase-mediated signaling pathways in JEV-infected cells. Some of these signaling pathways, including the AKT and ERK signaling pathways, have been reported to be activated in JEV-infected cells (*30*, *31*, *39*, *41*). Our findings support previous reports and extend the previous reports by identifying phosphoproteins that had not been previously associated with JEV infection and by identifying kinase pathways, such as the PKA pathway, as induced by JEV infection. PKA phosphorylates a large number of substrates involved in cell proliferation and inflammation (*42*, *43*) and plays various roles in the cellular response to viral infection and in viral replication and transmission. For instance, PKA is involved in the stimulation of IFN-α production in response to herpes simplex virus type 1 (*44*), HIV-1–associated PKA promotes viral genome reverse transcription (*45*), HCV infection activates PKA to promote virus release and transmission (*46*), and influenza A virus triggers *IL27* expression through PKA and adenosine 3′,5′-monophosphate (cAMP) response element–binding protein signaling (*47*). Through experiments with an inhibitor of PKA, our data indicated that PKA mediates proinflammatory signaling (induction of cytokines) in JEV-infected cells. Whether PKA has other roles in JEV infection remains to be determined, as do the downstream targets that mediate the PKA-dependent part of the inflammatory response.

Although we did not detect phosphopeptides corresponding to JNK1 in the phosphoproteomic data, we found that substrates of JNK1 were overrepresented among JEV infection–responsive upregulated phosphorylation sites and confirmed the activation of JNK1 and its substrate JUN, which was detected in the phosphoproteomics data, by Western blotting. Our study found that JEV genomic RNA contributes to JNK1 activation. Although endoplasmic reticulum (ER) stress can lead to activation of JNK signaling (*48*–*50*), and overexpression of JEV nonstructural proteins, such as NS1, NS2A, NS2B, and NS4B, triggers ER stress (*51*), we did not detect activation of JNK1 in glial cells overexpressing individual viral nonstructural proteins. This different response may be due to the different cell lines used in our study and in other studies. JEV infection causes the unfolded protein response (UPR) and apoptosis in baby hamster kidney cell line BHK-21 and the mouse neuroblastoma cell line N18, whereas UPR was not observed in response to JEV infection of the apoptosis-resistant cell line K562, a human erythroleukemic cell line (*48*–*50*), which suggested that UPR correlates with infection-induced apoptosis. However, JEV infection leads to activation but not apoptosis of glial cells both in vitro and in vivo (*4*, *6*, *11*), indicating

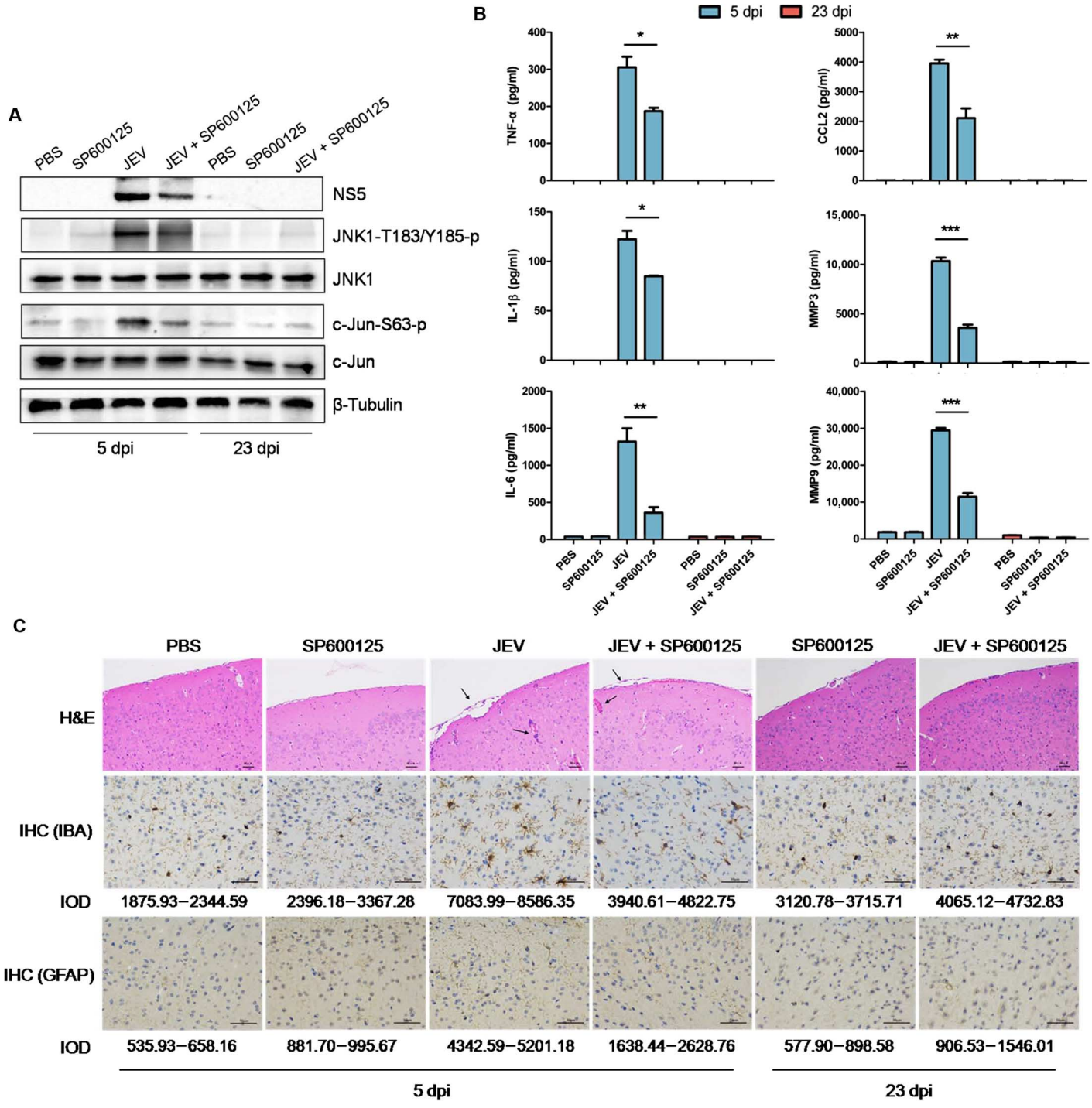

Fig. 8. JNK1 inhibitor treatment attenuates neuroinflammation in JEV-infected mouse model. Mice were subjected to the infection and treatment paradigm as described in Fig. 7A. (**A**) Phosphorylation of JNK1 and c-Jun was analyzed by Western blotting. dpi, days post-infection. (**B**) The concentrations of TNF-α, IL-1β, IL-6, and CCL2 in brain samples were determined by ELISA. Data were expressed as means ± SEM of three mice per group from three independent experiments. *$P < 0.05$, **$P < 0.01$, ***$P < 0.001$, Student's t test. (**C**) The histopathological changes of the mouse brain were observed by H&E staining. Meningitis and perivascular cuffing that appeared in the JEV-infected groups are indicated by arrows. Scale bars, 50 mm. Activation of microglia and astrocytes was detected by immunohistochemistry (IHC) using antibodies against ionized calcium-binding adaptor molecule 1 (IBA-1) and GFAP, respectively. Scale bars, 100 mm. Integrated option density (IOD) analysis was performed to quantify the results of staining. Data represent the ranges observed from three sections from three mice in each group.

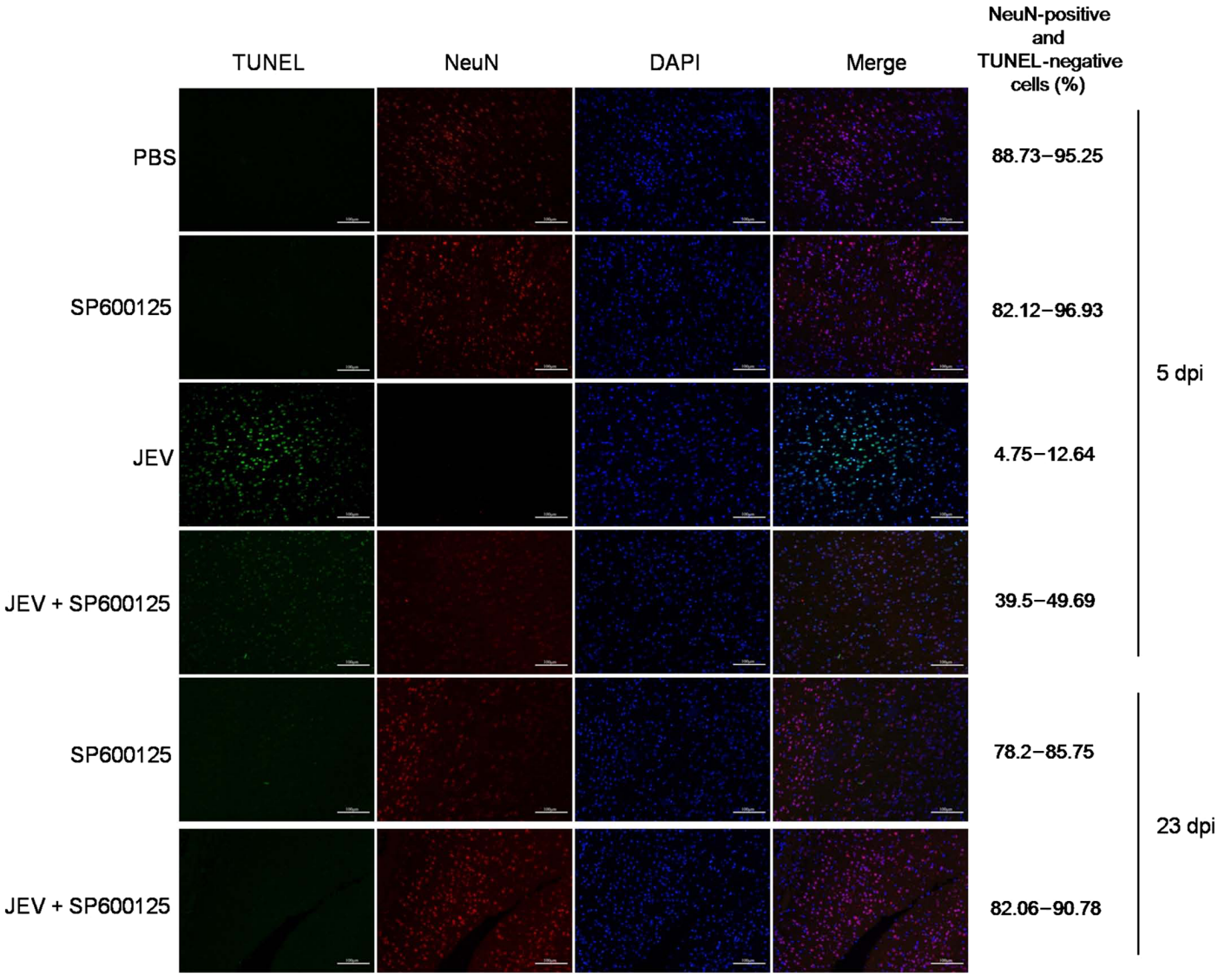

Fig. 9. JNK1 inhibitor treatment reduces neuronal death in JEV-infected mouse model. Mice were subjected to the infection and treatment paradigm as described in Fig. 7A. The apoptotic neurons in the brain sections were detected using the TUNEL Assay Kit (green), and neurons were detected with an antibody recognizing NeuN (red). Scale bars, 100 mm. The percentage of NeuN-positive and TUNEL-negative cells was determined. Data represent the ranges observed from three sections from three mice in each group.

that JEV infection or viral nonstructural proteins may not induce ER stress response in glial cells. However, we cannot exclude the possibility that viral proteins collectively contribute to JNK1 activation. Our data indicated that viral genomic RNA is sufficient to induce JNK1 activation.

JNK1 participates in many physiologic and pathologic processes and leads to phosphorylation of AP-1 subunits and activation of AP-1 transcriptional activity (*52*) to promote the expression of genes encoding proinflammatory cytokines (*53*, *54*). JNK signaling has a proinflammatory role in the pathogenesis of several inflammatory diseases that are not associated with infection, such as asthma (*55*), lung inflammation (*56*), rheumatoid arthritis (*57*, *58*), and neuropathic pain (*59*). In case of viral infection, activation of JNK signaling promotes enterovirus 71 infection in immature dendritic cells (*60*). Inhibition of JNK signaling reduced the lipopolysaccharide-induced increase in metabolic activity of microglial cells and induction of the AP-1 target genes encoding cyclooxygenase-2, TNF-α, MCP-1, and IL-6 (*61*). Potentially important for JEV infection and infection with other neurotropic viruses, JNK signaling promotes expression of MMP-encoding genes, which may contribute to the disruption of the blood-brain barrier during JEV infection (*39*).

Several selective JNK chemical inhibitors have been developed (*62*). Some of which have exhibited efficacy in ameliorating some symptoms of different diseases in animal models (*55*, *63*, *64*), and some inhibitors exhibit anti-inflammatory properties (*65*). SP600125 is a potent, cell-permeable, reversible adenosine triphosphate competitive inhibitor for JNK with >20-fold selectivity versus a range of kinases and enzymes tested (*66*). It specifically blocks JNK, but not other inflammatory signaling cascades, and has been widely used in animal models (*55*, *63*, *64*, *66*). In rats, SP600125 induces neuroprotection against ischemic brain injury by suppressing the extrinsic and intrinsic

pathways of apoptosis, which supports the application of SP600125 in neurological diseases (*63*). Peripheral administration of SP600125 to mice prevents the changes induced by methamphetamine in MMP activity, laminin protein abundance, and disruption of the blood-brain barrier, indicating that SP600125 penetrates into the CNS (*67*). Here, exposing glial cells in culture to the JNK inhibitor SP600125 suppressed the activation of JNK1 and JUN during JEV infection and reduced JEV-induced inflammatory cytokines, suggesting that JNK1 plays an important role in the JEV-induced inflammatory response of glial cells. We also found a reduction of JNK1 and JUN phosphorylation in the JEV-infected mouse brain in animals treated with intravenous injection of SP600125, confirming the inhibitory effect of SP600125 on JNK1 signaling. Mice treated with SP600125 showed a significant reduction in the secretion of proinflammatory cytokines, along with the alleviation of histopathological symptoms, less glial activation, and reduced neuronal cell death during JEV infection. In addition, treatment of SP600125 rescued 40% of mice with well-established JEV infection. These results further support the crucial role of JNK1 signaling in JEV-induced neuroinflammation and suggest the clinical importance of JNK1 in the disease. SP600125 treatment also reduced the viral load in the mouse brain, suggesting that SP600125 may alleviate the symptoms of JE not only due to the inhibition of inflammatory response but also due to the reduced viral replication in the brain. However, this phenomenon seems unlikely to be a result of direct antiviral activity of SP600125 because we did not detect any alteration of viral titers in JEV-infected U251 cells or BV-2 cells upon SP600125 treatment. Therefore, we propose that the SP600125-related reduction of viral load in the mouse brain resulted from the improved inflammatory environment by enabling more effective clearance of the virus.

Because the outcome of JEV pathogenesis is influenced by inflammatory mediators, which triggers bystander damage to neurons (*11*), the inhibition of inflammatory signaling in the CNS should be beneficial in treating the effects of JEV infection. Previously, we showed that the inhibition of TNF-α signaling by etanercept reduced neuroinflammation and lethality during JEV infection in mice (*68*). We have also shown that suppression of the inflammation-related miRNAs, miR-15b and miR-19b-3p, using specific antagomirs provides protection against JEV-induced acute encephalitis in mice (*13*, *14*). Similarly, our previous studies and several other studies also demonstrated that inhibition of neuroinflammation during JEV infection by treatment of etanercept (*68*), antagomir-15b (*13*), antagomir-19b-3p (*14*), minocycline (a broad-spectrum tetracycline antibiotic that is protective in neurological disease models associated with inflammation) (*69*, *70*), or rosmarinic acid (a plant-derived compound with anti-inflammatory properties) can reduce viral load in the mouse brain (*71*). Future studies will establish whether combinations of drugs provide the best therapeutic effects or whether patients should be stratified into different treatment groups.

Because JEV and WNV are closely related and both can cause an inflammatory response in the CNS, comparison of the respective phosphoproteomes of JEV- or WNV-infected cells identified 459 phosphopeptides that were regulated by either virus, suggesting that JEV and WNV induce multiple common host molecular processes in infected cells. Again, JNK1 was also the most overrepresented kinase in U251 cells infected with WNV, indicating that JNK1 may also play a critical role in WNV-induced inflammation. This analysis provides a large-scale comparison of host signaling after infection by different flaviviruses, and the identification of new co-regulated host pathways may facilitate the development of broad-spectrum drugs for treating both JEV and WNV infection.

In summary, we demonstrated through our phosphoproteomic approach that multiple kinase-mediated signaling pathways are activated in JEV-infected glial cells. Our in vitro and in vivo functional studies revealed that JNK1 plays a pivotal role in JEV-induced inflammation in the CNS and could be a therapeutic target for this disease. The phosphoproteomic data provide a valuable resource for understanding the response to flavivirus infection and for exploring novel therapeutic targets for JEV infection.

MATERIALS AND METHODS

Cell culture and virus propagation

Human glioma cell line U251 (also known as human glioblastoma or astrocytoma cell line) and mouse microglial cell line BV-2 were cultured and maintained in Dulbecco's modified Eagle's medium (DMEM; 4500 mg/liter glucose) supplemented with 10% (v/v) heat-inactivated fetal bovine serum, penicillin (100 U/ml), and streptomycin sulfate (100 μg/ml) at 37°C in a 5% CO_2 atmosphere. JEV wild-type strain P3 was propagated in suckling mouse brains, and the titer of the virus was determined by plaque assay on BHK-21 cells.

Immunofluorescence assay

After the cells were grown to 80% confluency, nonadherent cells were removed by washing with medium before virus inoculation. The cells were mock-infected or infected with JEV P3 strain at an MOI of 1, 2, or 5 for 1 hour. The mock-infected cells were prepared using the same procedures but omitting the viral infection. At 12 and 36 hours after infection, cells were fixed and blocked with 10% bovine serum albumin (BSA) in PBS (pH 7.2) for 30 min. Then, cells were stained with the monoclonal antibody recognizing JEV NS5 (5 ng/μl for immunofluorescence assay, prepared by our laboratory) for 1 hour. After washing three times with PBS, cells were incubated with Alexa Fluor 488–conjugated secondary antibody (Invitrogen) for 30 min. Cell nuclei were stained with DAPI (Invitrogen). The staining was observed using a fluorescence microscope (Zeiss) with 20× magnification.

RNA extraction and qRT-PCR

Total RNA was extracted from treated cells with TRIzol reagent (Invitrogen) according to the manufacturer's instructions, and 1 mg of RNA was used to synthesize complementary DNA (cDNA) with a first-strand cDNA Synthesis Kit (TOYOBO). qRT-PCR analysis was performed using a 7500 Real-time PCR System (Applied Biosystems) and SYBR Green Real-time PCR Master Mix (TOYOBO). Data were normalized according to the amount of β-actin expression in each sample.

Virus infection and protein hydrolysis and digestion

After the cells were grown to 80% confluency, nonadherent cells were removed by washing with medium before virus inoculation. The cells were infected with JEV P3 strain at an MOI of 5 for 1 hour and then harvested at 12 hours after infection. The mock-infected cells were prepared using the same procedures but omitting the viral infection. The harvested cells were centrifuged at 3000*g* for 5 min and washed three times with cold PBS. The cells were lysed in lysis buffer [1 mM phenylmethylsulfonyl fluoride, 1% (w/v) SDS, 2 mM EDTA, 5 mM α-glycerophosphate, 10 mM NaF, 10 mM dithiothreitol (DTT), and 100 mM sodium pyrophosphate decahydrate]. Lysis debris was removed by centrifugation at 25,000*g* for 20 min. Sample reduction and alkylation were performed with an additional amount

of 10 mM DTT and 55 mM iodoacetamide, respectively, at room temperature. After centrifugation at 5000*g* for 20 min, the precipitate was washed twice with 80% (v/v) ice-cold acetone, dried under vacuum, and then suspended in 0.5 M triethylammonium bicarbonate. The concentration of supernatant protein was quantified by using the Bradford assay, and those proteins were then digested with sequencing grade modified trypsin (Promega; 10 g of trypsin per milligram of protein) for 16 hours at 37°C. Peptides were desalted on a C18 Sep-Pak cartridge (Waters) and dried under vacuum. Peptide was eluted with 3.5% (v/v) trifluoroacetic acid (TFA)/65% (v/v) acetonitrile solution saturated with glutamic acid.

Phosphopeptide enrichment

Phosphopeptides were enriched using TiO_2, as previously described (*72*). Briefly, 500 g of TiO_2 (GL Sciences) and 1 mg of the phosphopeptides were mixed and then incubated for 20 min with end-over-end rotation. The mixture was first washed with 0.5% (v/v) TFA/65% (v/v) acetonitrile and then with 0.1% (v/v) TFA/65% (v/v) acetonitrile. The phosphopeptides were eluted with 0.3 M NH_4OH/50% (v/v) acetonitrile and dried under vacuum.

Liquid chromatography–tandem mass spectrometry

TiO_2-enriched phosphopeptides were resuspended in buffer A (high-performance liquid chromatography–grade water, 2% acetonitrile, and 0.5% acetic acid), whereby 1 μg of digested protein (10 μl) was injected per LC-MS/MS run. Each of the samples was run in triplicate. The trap column effluent was transferred to a reversed-phase microcapillary column (0.075 × 150 mm, Acclaim PepMap100 C18 column, 3 μm, 100 Å; Dionex). Reversed-phase separation of peptides was performed using buffer A (2% acetonitrile and 0.5% acetic acid) and buffer B (80% acetonitrile and 0.5% acetic acid) under a 238-min gradient (4 to 30% buffer B for 208 min, 30 to 45% buffer B for 20 min, 45 to 100% buffer B for 1 min, 100% buffer B for 8 min, and 100 to 4% buffer B for 1 min). An MS survey scan was obtained for the mass-to-charge ratio (*m/z*) range 350 to 1800, and MS/MS spectra were acquired in the LTQ for the 20 most intense ions from the survey scan (determined using Xcalibur mass spectrometer software in real time). A precursor MS scan of each intact phosphopeptide was recorded using an LTQ-Orbitrap Velos spectrometer (Thermo Fisher Scientific) from 350 to 2000 *m/z*. The eight most intense multiply charged precursor ions were subjected to collision-induced dissociation for 30 ms at a normalized collision energy of 35.0. The automatic gain control targets were 10,000 ions for the MS/MS scans and 100,000 for the Orbitrap scans. A dynamic exclusion time (30 s) was applied to avoid repeated analysis of the same component.

Data processing and analysis

The raw MS data were analyzed using Progenesis LC-MS software (version 4.1, Nonlinear Dynamics). Quantification was performed for each condition after automatic retention time calibration, peak detection, and normalization in Progenesis LC-MS. The peak list was created by Progenesis LC-MS and searched in Mascot (version 2.4.1, Matrixscience). The decoy option was turned on in Mascot. The following search parameters were included: a fragment mass tolerance of 0.6 Da, a peptide mass tolerance of 10 parts per million, and a maximum of two missed trypsin cleavages. The program also searched for carboxyamidomethylated Cys, which was a required modified residue, and deamidated Asn and Gln, N-terminal acetyl groups, oxidized Met, N-terminal pyro-Glu, and phosphorylated Ser, Thr, and Tyr, which were allowed modified residues. Results were analyzed with ProteinPilot software (version 4.0, SCIEX) with a peptide probability value set to 95%. A 5% false discovery rate on peptide level was applied. All confident phosphopeptides were exported and quantified with Progenesis LC-MS. For comparison between samples, we chose a twofold cutoff to consider peptides as increased in phosphorylation and a 0.5-fold cutoff to consider peptides as decreased in phosphorylation. The confidence value of each phosphorylation site was calculated using the A-score algorithm. A cutoff value of 90% confidence was adjusted to select differentially expressed phosphopeptides that met the high site confidence threshold. The Uniprot Sus scrofa (released March 2015) and IPI human database (ftp://ftp.ebi.ac.uk/pub/databases/IPI) were used for protein identification.

Immunoblotting

Cell pellets or mouse brain tissue were lysed in radioimmunoprecipitation assay buffer (Sigma) containing phosphatase (PhosSTOP, Roche) and protease inhibitors (cOmplete Tablets, Roche). Protein concentrations were measured using BCA (bicinchoninic acid) Protein Assay Kit reagents (Thermo Fisher Scientific). Each sample was electrophoresed and transferred onto a nitrocellulose membrane. Membranes were then blocked by incubation in blocking buffer (tris-buffered saline with 0.5% Tween 20 and 5% BSA) for 1 hour and probed with primary antibodies. After washing, membranes were incubated with the appropriate peroxidase-conjugated secondary antibodies (Boster). The blots were processed for development using SuperSignal West Femto (Thermo Fisher Scientific). The primary antibodies used were as follows: mouse monoclonal antibody against JEV NS5 (1 ng/μl for Western blot assay, prepared by our laboratory) (*73*), rabbit polyclonal antibodies against AKT-1, phosphor-AKT-1-Ser124, PRKACA, phosphor-PRKACA-T198, p53, JNK1, c-Jun, phosphor-c-Jun-S63, and β-tubulin (ABclonal Technology), and rabbit polyclonal antibodies against phosphor-p53-Ser392 and phosphor-JNK1-Thr183/185 (Cell Signaling Technology). Appropriate concentrations for these commercial antibodies were used following the manufacturer's guidelines.

Inhibitor or activator treatment

U251 and BV-2 cells were treated with various pharmacological compounds dissolved in DMSO: AKT inhibitor (API-59CJ-OMe, 12 μM; Calbiochem-Merck), PKA inhibitor (H89, 30 μM; Selleckchem), JNK inhibitor (SP600125, 5 μM; Selleckchem), and TP53 activator (JNJ-26854165, 10 μM; Selleckchem). Cells were exposed to the inhibitors for the times indicated and then infected with JEV. Cells for negative control were treated with DMSO in equal volume.

Plasmid construction and RNA interference

To construct the JNK1 expression plasmid, we amplified the coding regions from cDNA derived from HeLa cells by PCR and cloned into pcDNA3.1 to yield pcDNA-JNK1. siRNAs targeting JNK1 (5′-AAGCCCAGUAAUAUAGUAGUA-3′) and JUN (5′-GAAAGUCAUGAACCACGUU-3′) and the nonspecific control siRNA were purchased from GenePharma. Transfection was performed with Lipofectamine 2000 (Invitrogen). Cells were transfected with each siRNA (50 nM).

In vitro transcription of JEV replicon and replication analysis

The plasmid carrying the JEV subgenomic replicon or empty vector was transcribed in vitro using the T7 MEGAscript Kit (Ambion)

according to the manufacturer's instructions. The transcribed RNA was transfected into U251 cells using the Lipofectamine 2000 (Invitrogen). The cells were harvested at 0, 6, 12, and 18 hours after transfection, and the replication of JEV replicon was analyzed by qRT-PCR and Western blotting of NS5.

Enzyme-linked immunosorbent assay

The culture supernatants were collected from treated cells at the indicated time points and stored at −80°C. The mouse brain tissues were homogenized in DMEM and stored at −80°C. Before ELISA, the mouse brain samples were thawed and centrifuged at 5000*g*, and the supernatants were collected. The protein concentrations of TNF-α, IL-1β, IL-6, CCL2, MMP3, and MMP9 in cell cultures or mouse brain tissue lysates were measured with ELISA kits, following the manufacturer's instructions. TNF-α, IL-1β, IL-6, and CCL2 ELISA kits were purchased from eBioscience; MMP3 and MMP9 ELISA kits were purchased from Elabscience.

JEV challenge and inhibitor administration

Adult BALB/c mice (6 weeks old) were purchased from the Hubei Provincial Center for Disease Control and Prevention (Wuhan, China). Mice were randomly assigned to four groups ($n = 15$ per group): group 1, control group (PBS); group 2, the SP600125-treated group (SP600125); group 3, the JEV-infected group (JEV); and group 4, the JEV-infected and SP600125-treated group (JEV + SP600125). Mice in groups 1 and 2 were inoculated intracranially with 20 ml of PBS, whereas mice in groups 3 and 4 were injected intracranially with 50 PFU of JEV P3 strain in 20 ml of PBS. Three and four days after infection, mice in groups 2 and 4 were injected intravenously with SP600125 (15 mg/kg body weight, in 10% DMSO in PBS), and mice in group 3 were injected intravenously with equal volume of 10% DMSO. After 5 days, mice infected with JEV developed signs of viral encephalitis; five mice in each group were killed, and brain samples were collected for further studies. Ten remaining mice were monitored daily to assess behavior and mortality. All animal experiments were performed in accordance with the National Institutes of Health's *Guide for the Care and Use of Laboratory Animals*, and the experimental protocols were approved by the Huazhong Agricultural University's Research Ethics Committee of the College of Veterinary Medicine (no. 42000600010004).

H&E staining and immunohistochemistry and TUNEL assay

Mice were anesthetized with ketamine-xylazine (0.1 ml per 10 g of body weight) and perfused with PBS, followed by 4% paraformaldehyde. Brain tissues were removed and embedded in paraffin for coronal sections. The standard H&E staining protocol was followed for tissue staining. For immunohistochemical staining, sections were incubated overnight at 4°C with primary antibodies against IBA-1 (Wako), GFAP (Dako), and NeuN (Chemi-Con) at the concentrations indicated in the manufacturer's guidelines. After washing, slides were incubated with anti-mouse horseradish peroxidase–conjugated secondary antibodies and washed, and 3,3′-diaminobenzidine (Vector Laboratories) was used for color development. For TUNEL, an In Situ Cell Death Detection Kit (Roche) was used according to the manufacturer's instructions.

Statistical analysis

All experiments were carried out at least three times with similar results. Analyses were conducted using Prism 5 (GraphPad Software). Results are expressed as means ± SEM. Data were compared with two-way ANOVA with subsequent Bonferroni post test for multiple comparisons or with Student's *t* test. For all tests, $P < 0.05$ was considered significant.

SUPPLEMENTARY MATERIALS

www.sciencesignaling.org/cgi/content/full/9/448/ra98/DC1

Fig. S1. Expression of inflammatory cytokines in JEV-infected U251 cells.
Fig. S2. Protein-protein interaction network constructed from the phosphoproteins regulated by JEV infection of U251 cells.
Fig. S3. Representative MS of phosphorylated peptides of AKT1, PRKACA, and TP53.
Table S1. Quantification of phosphopeptides detected by LC-MS/MS.
Table S2. Differentially regulated phosphopeptides in response to JEV infection.
Table S3. GO and KEGG pathway analysis of the up-regulated phosphoproteome of JEV-infected U251 cells.
Table S4. GO and KEGG pathway analysis of the down-regulated phosphoproteome of JEV-infected U251 cells.
Table S5. Phosphoproteins in the interaction network of JEV-infected U251 cells.
Table S6. Differentially regulated phosphoproteins that are shared between cells infected with JEV or WNV.
Table S7. Prediction of JEV-responsive kinases by using the GPS.
Table S8. Overrepresented motifs in the up-regulated phosphoproteins in JEV-infected cells.

REFERENCES AND NOTES

1. G. L. Campbell, S. L. Hills, M. Fischer, J. A. Jacobson, C. H. Hoke, J. M. Hombach, A. A. Marfin, T. Solomon, T. F. Tsai, V. D. Tsu, A. S. Ginsburg, Estimated global incidence of Japanese encephalitis: A systematic review. *Bull. World Health Organ.* **89**, 766E–774E (2011).
2. S.-I. Yun, Y.-M. Lee, Japanese encephalitis: The virus and vaccines. *Hum. Vaccin. Immunother.* **10**, 263–279 (2014).
3. U. K. Misra, J. Kalita, Overview: Japanese encephalitis. *Prog. Neurobiol.* **91**, 108–120 (2010).
4. A. Ghoshal, S. Das, S. Ghosh, M. K. Mishra, V. Sharma, P. Koli, E. Sen, A. Basu, Proinflammatory mediators released by activated microglia induces neuronal death in Japanese encephalitis. *Glia* **55**, 483–496 (2007).
5. M. Diagana, P.-M. Preux, M. Dumas, Japanese encephalitis revisited. *J. Neurol. Sci.* **262**, 165–170 (2007).
6. C.-J. Chen, S.-L. Liao, M.-D. Kuo, Y.-M. Wang, Astrocytic alteration induced by Japanese encephalitis virus infection. *Neuroreport* **11**, 1933–1937 (2000).
7. J. K. Olson, S. D. Miller, Microglia initiate central nervous system innate and adaptive immune responses through multiple TLRs. *J. Immunol.* **173**, 3916–3924 (2004).
8. A. S. Harms, J.-K. Lee, T. A. Nguyen, J. Chang, K. M. Ruhn, I. Treviño, M. G. Tansey, Regulation of microglia effector functions by tumor necrosis factor signaling. *Glia* **60**, 189–202 (2012).
9. J. A. Smith, A. Das, S. K. Ray, N. L. Banik, Role of pro-inflammatory cytokines released from microglia in neurodegenerative diseases. *Brain Res. Bull.* **87**, 10–20 (2012).
10. A. Vezzani, T. Granata, Brain inflammation in epilepsy: Experimental and clinical evidence. *Epilepsia* **46**, 1724–1743 (2005).
11. C.-J. Chen, Y.-C. Ou, S.-Y. Lin, S.-L. Raung, S.-L. Liao, C.-Y. Lai, S.-Y. Chen, J.-H. Chen, Glial activation involvement in neuronal death by Japanese encephalitis virus infection. *J. Gen. Virol.* **91**, 1028–1037 (2010).
12. R. Jiang, J. Ye, B. Zhu, Y. Song, H. Chen, S. Cao, Roles of TLR3 and RIG-I in mediating the inflammatory response in mouse microglia following Japanese encephalitis virus infection. *J. Immunol. Res.* **2014**, 787023 (2014).
13. B. Zhu, J. Ye, Y. Nie, U. Ashraf, A. Zohaib, X. Duan, Z. F. Fu, Y. Song, H. Chen, S. Cao, MicroRNA-15b modulates Japanese encephalitis virus–mediated inflammation via targeting RNF125. *J. Immunol.* **195**, 2251–2262 (2015).
14. U. Ashraf, B. Zhu, J. Ye, S. Wan, Y. Nie, Z. Chen, M. Cui, C. Wang, X. Duan, H. Zhang, H. Chen, S. Cao, MicroRNA-19b-3p modulates Japanese encephalitis virus-mediated inflammation via targeting RNF11. *J. Virol.* **90**, 4780–4795 (2016).
15. Y. Yang, J. Ye, X. Yang, R. Jiang, H. Chen, S. Cao, Japanese encephalitis virus infection induces changes of mRNA profile of mouse spleen and brain. *Virol. J.* **8**, 80 (2011).
16. L.-K. Zhang, F. Chai, H.-Y. Li, G. Xiao, L. Guo, Identification of host proteins involved in Japanese encephalitis virus infection by quantitative proteomics analysis. *J. Proteome Res.* **12**, 2666–2678 (2013).
17. G.-R. Yan, Q.-Y. He, Functional proteomics to identify critical proteins in signal transduction pathways. *Amino Acids* **35**, 267–274 (2008).

18. C. Choudhary, M. Mann, Decoding signalling networks by mass spectrometry-based proteomics. *Nat. Rev. Mol. Cell Biol.* **11**, 427–439 (2010).
19. B. Macek, M. Mann, J. V. Olsen, Global and site-specific quantitative phosphoproteomics: Principles and applications. *Annu. Rev. Pharmacol. Toxicol.* **49**, 199–221 (2009).
20. V. Ravikumar, C. Jers, I. Mijakovic, Elucidating host–pathogen interactions based on post-translational modifications using proteomics approaches. *Front. Microbiol.* **6**, 1313 (2015).
21. J. A. Wojcechowskyj, C. A. Didigu, J. Y. Lee, N. F. Parrish, R. Sinha, B. H. Hahn, F. D. Bushman, S. T. Jensen, S. H. Seeholzer, R. W. Doms, Quantitative phosphoproteomics reveals extensive cellular reprogramming during HIV-1 entry. *Cell Host Microbe* **13**, 613–623 (2013).
22. R. Luo, L. Fang, H. Jin, D. Wang, K. An, N. Xu, H. Chen, S. Xiao, Label-free quantitative phosphoproteomic analysis reveals differentially regulated proteins and pathway in PRRSV-infected pulmonary alveolar macrophages. *J. Proteome Res.* **13**, 1270–1280 (2014).
23. H. Zhang, J. Sun, J. Ye, U. Ashraf, Z. Chen, B. Zhu, W. He, Q. Xu, Y. Wei, H. Chen, Z. F. Fu, R. Liu, S. Cao, Quantitative label-free phosphoproteomics reveals differentially regulated protein phosphorylation involved in West Nile virus-induced host inflammatory response. *J. Proteome Res.* **14**, 5157–5168 (2015).
24. P. M. Kulkarni, E. Barton, M. Savelonas, R. Padmanabhan, Y. Lu, K. Trett, W. Shain, J. L. Leasure, B. Roysam, Quantitative 3-D analysis of GFAP labeled astrocytes from fluorescence confocal images. *J. Neurosci. Methods* **246**, 38–51 (2015).
25. M. Kanehisa, S. Goto, KEGG: Kyoto encyclopedia of genes and genomes. *Nucleic Acids Res.* **28**, 27–30 (2000).
26. S. Gupta, T. Barrett, A. J. Whitmarsh, J. Cavanagh, H. K. Sluss, B. Dérijard, R. J. Davis, Selective interaction of JNK protein kinase isoforms with transcription factors. *EMBO J.* **15**, 2760–2770 (1996).
27. B. Dérijard, M. Hibi, I.-H. Wu, T. Barrett, B. Su, T. Deng, M. Karin, R. J. Davis, JNK1: A protein kinase stimulated by UV light and Ha-Ras that binds and phosphorylates the c-Jun activation domain. *Cell* **76**, 1025–1037 (1994).
28. D. Schwartz, S. P. Gygi, An iterative statistical approach to the identification of protein phosphorylation motifs from large-scale data sets. *Nat. Biotechnol.* **23**, 1391–1398 (2005).
29. G. Manning, D. B. Whyte, R. Martinez, T. Hunter, S. Sudarsanam, The protein kinase complement of the human genome. *Science* **298**, 1912–1934 (2002).
30. N. Gupta, A. S. Bala Bhaskar, P. V. Lakshmana Rao, Transcriptional regulation and activation of the mitogen-activated protein kinase pathway after Japanese encephalitis virus infection in neuroblastoma cells. *FEMS Immunol. Med. Microbiol.* **62**, 110–121 (2011).
31. T.-C. Yang, C.-C. Lai, S.-L. Shiu, P.-H. Chuang, B.-C. Tzou, Y.-Y. Lin, F.-J. Tsai, C.-W. Lin, Japanese encephalitis virus down-regulates thioredoxin and induces ROS-mediated ASK1-ERK/p38 MAPK activation in human promonocyte cells. *Microbes Infect.* **12**, 643–651 (2010).
32. Y. Fleming, C. G. Armstrong, N. Morrice, A. Paterson, M. Goedert, P. Cohen, Synergistic activation of stress-activated protein kinase 1/c-Jun N-terminal kinase (SAPK1/JNK) isoforms by mitogen-activated protein kinase kinase 4 (MKK4) and MKK7. *Biochem. J.* **352** (Pt. 1), 145–154 (2000).
33. G. Song, G. Ouyang, S. Bao, The activation of Akt/PKB signaling pathway and cell survival. *J. Cell. Mol. Med.* **9**, 59–71 (2005).
34. S. Leppä, D. Bohmann, Diverse functions of JNK signaling and c-Jun in stress response and apoptosis. *Oncogene* **18**, 6158–6162 (1999).
35. M. J. Moore, J. R. Kanter, K. C. Jones, S. S. Taylor, Phosphorylation of the catalytic subunit of protein kinase A. Autophosphorylation versus phosphorylation by phosphoinositide-dependent kinase-1. *J. Biol. Chem.* **277**, 47878–47884 (2002).
36. M. G. Luciani, J. R. A. Hutchins, D. Zheleva, T. R. Hupp, The C-terminal regulatory domain of p53 contains a functional docking site for cyclin A. *J. Mol. Biol.* **300**, 503–518 (2000).
37. S. Goda, Y. Kato, E. Domae, H. Hayashi, N. Tani-Ishii, J. Iida, T. Ikeo, Effects of JNK1/2 on the inflammation cytokine TNF-α-enhanced production of MMP-3 in human dental pulp fibroblast-like cells. *Int. Endod. J.* **48**, 1122–1128 (2015).
38. W.-H. Tung, H.-W. Tsai, I.-T. Lee, H.-L. Hsieh, W.-J. Chen, Y.-L. Chen, C.-M. Yang, Japanese encephalitis virus induces matrix metalloproteinase-9 in rat brain astrocytes via NF-κB signalling dependent on MAPKs and reactive oxygen species. *Br. J. Pharmacol.* **161**, 1566–1583 (2010).
39. C.-M. Yang, C.-C. Lin, I.-T. Lee, Y.-H. Lin, C.-M. Yang, W.-J. Chen, M.-J. Jou, L.-D. Hsiao, Japanese encephalitis virus induces matrix metalloproteinase-9 expression via a ROS/c-Src/PDGFR/PI3K/Akt/MAPKs-dependent AP-1 pathway in rat brain astrocytes. *J. Neuroinflammation* **9**, 12 (2012).
40. D. Leppert, R. L. P. Lindberg, L. Kappos, S. L. Leib, Matrix metalloproteinases: Multifunctional effectors of inflammation in multiple sclerosis and bacterial meningitis. *Brain Res. Brain Res. Rev.* **36**, 249–257 (2001).
41. S. Das, S. Chakraborty, A. Basu, Critical role of lipid rafts in virus entry and activation of phosphoinositide 3′ kinase/Akt signaling during early stages of Japanese encephalitis virus infection in neural stem/progenitor cells. *J. Neurochem.* **115**, 537–549 (2010).
42. W.-Z. Ran, L. Dong, C.-Y. Tang, Y. Zhou, G.-Y. Sun, T. Liu, Y.-P. Liu, C.-X. Guan, Vasoactive intestinal peptide suppresses macrophage-mediated inflammation by downregulating interleukin-17A expression via PKA- and PKC-dependent pathways. *Int. J. Exp. Pathol.* **96**, 269–275 (2015).
43. T. Zhu, X. I. Wu, W. Zhang, M. Xiao, Glucagon like peptide-1 (GLP-1) modulates OVA-induced airway inflammation and mucus secretion involving a protein kinase A (PKA)-dependent nuclear factor-κB (NF-κB) signaling pathway in mice. *Int. J. Mol. Sci.* **16**, 20195–20211 (2015).
44. Q. Li, M. Feldman, C. Harmon, P. Fitzgerald-Bocarsly, Role of tyrosine kinases, protein kinase C, and protein kinase A in the regulation of interferon-α production induced by herpes simplex virus type 1. *J. Interferon Cytokine Res.* **16**, 109–118 (1996).
45. C. Giroud, N. Chazal, B. Gay, P. Eldin, S. Brun, L. Briant, HIV-1-associated PKA acts as a cofactor for genome reverse transcription. *Retrovirology* **10**, 157 (2013).
46. M. J. Farquhar, H. J. Harris, M. Diskar, S. Jones, C. J. Mee, S. U. Nielsen, C. L. Brimacombe, S. Molina, G. L. Toms, P. Maurel, J. Howl, F. W. Herberg, S. C. D. van Ijzendoorn, P. Balfe, J. A. McKeating, Protein kinase A-dependent step(s) in hepatitis C virus entry and infectivity. *J. Virol.* **82**, 8797–8811 (2008).
47. L. Liu, Z. Cao, J. Chen, R. Li, Y. Cao, C. Zhu, K. Wu, J. Wu, F. Liu, Y. Zhu, Influenza A virus induces interleukin-27 through cyclooxygenase-2 and protein kinase A signaling. *J. Biol. Chem.* **287**, 11899–11910 (2012).
48. M. Huang, A. Xu, X. Wu, Y. Zhang, Y. Guo, F. Guo, Z. Pan, L. Kong, Japanese encephalitis virus induces apoptosis by the IRE1/JNK pathway of ER stress response in BHK-21 cells. *Arch. Virol.* **161**, 699–703 (2016).
49. Y.-P. Wu, C.-M. Chang, C.-Y. Hung, M.-C. Tsai, S. C. Schuyler, R. Y.-L. Wang, Japanese encephalitis virus co-opts the ER-stress response protein GRP78 for viral infectivity. *Virol. J.* **8**, 128 (2011).
50. H.-L. Su, C.-L. Liao, Y.-L. Lin, Japanese encephalitis virus infection initiates endoplasmic reticulum stress and an unfolded protein response. *J. Virol.* **76**, 4162–4171 (2002).
51. C.-Y. Yu, Y.-W. Hsu, C.-L. Liao, Y.-L. Lin, Flavivirus infection activates the XBP1 pathway of the unfolded protein response to cope with endoplasmic reticulum stress. *J. Virol.* **80**, 11868–11880 (2006).
52. S. Morton, R. J. Davis, A. McLaren, P. Cohen, A reinvestigation of the multisite phosphorylation of the transcription factor c-Jun. *EMBO J.* **22**, 3876–3886 (2003).
53. X. Lu, L. Ma, L. Ruan, Y. Kong, H. Mou, Z. Zhang, Z. Wang, J. M. Wang, Y. Le, Resveratrol differentially modulates inflammatory responses of microglia and astrocytes. *J. Neuroinflammation* **7**, 46 (2010).
54. P. Nath, P. Eynott, S.-Y. Leung, I. M. Adcock, B. L. Bennett, K. F. Chung, Potential role of c-Jun NH_2-terminal kinase in allergic airway inflammation and remodelling: Effects of SP600125. *Eur. J. Pharmacol.* **506**, 273–283 (2005).
55. H.-M. Wu, L. Fang, Q.-Y. Shen, R.-Y. Liu, SP600125 promotes resolution of allergic airway inflammation via TLR9 in an OVA-induced murine acute asthma model. *Mol. Immunol.* **67**, 311–316 (2015).
56. J. Van der Velden, Y. M. W. Janssen-Heininger, S. Mandalapu, E. V. Scheller, J. K. Kolls, J. F. Alcorn, Differential requirement for c-Jun N-terminal kinase 1 in lung inflammation and host defense. *PLOS ONE* **7**, e34638 (2012).
57. D. de Launay, M. G. van de Sande, M. J. de Hair, A. M. Grabiec, G. P. van de Sande, K. A. Lehmann, C. A. Wijbrandts, L. G. van Baarsen, D. M. Gerlag, P. P. Tak, K. A. Reedquist, Selective involvement of ERK and JNK mitogen-activated protein kinases in early rheumatoid arthritis (1987 ACR criteria compared to 2010 ACR/EULAR criteria): A prospective study aimed at identification of diagnostic and prognostic biomarkers as well as therapeutic targets. *Ann. Rheum. Dis.* **71**, 415–423 (2012).
58. M. Guma, G. S. Firestein, c-Jun N-terminal kinase in inflammation and rheumatic diseases. *Open Rheumatol. J.* **6**, 220–231 (2012).
59. J. Cao, J.-s. Wang, X.-h. Ren, W.-d. Zang, Spinal sample showing p-JNK and P38 associated with the pain signaling transduction of glial cell in neuropathic pain. *Spinal Cord* **53**, 92–97 (2015).
60. H. Peng, M. Shi, L. Zhang, Y. Li, J. Sun, L. Zhang, X. Wang, X. Xu, X. Zhang, Y. Mao, Y. Ji, J. Jiang, W. Shi, Activation of JNK1/2 and p38 MAPK signaling pathways promotes enterovirus 71 infection in immature dendritic cells. *BMC Microbiol.* **14**, 147 (2014).
61. H. Zhao, L. Cheng, Y. Liu, W. Zhang, S. Maharjan, Z. Cui, X. Wang, D. Tang, L. Nie, Mechanisms of anti-inflammatory property of conserved dopamine neurotrophic factor: Inhibition of JNK signaling in lipopolysaccharide-induced microglia. *J. Mol. Neurosci.* **52**, 186–192 (2014).
62. P. Koch, M. Gehringer, S. A. Laufer, Inhibitors of c-Jun N-terminal kinases: An update. *J. Med. Chem.* **58**, 72–95 (2015).
63. Q.-H. Guan, D.-S. Pei, X.-M. Liu, X.-T. Wang, T.-L. Xu, G.-Y. Zhang, Neuroprotection against ischemic brain injury by SP600125 via suppressing the extrinsic and intrinsic pathways of apoptosis. *Brain Res.* **1092**, 36–46 (2006).
64. Y. Zheng, M. Zhang, Y. Zhao, J. Chen, B. Li, W. Cai, JNK inhibitor SP600125 protects against lipopolysaccharide-induced acute lung injury via upregulation of claudin-4. *Exp. Ther. Med.* **8**, 153–158 (2014).

65. S. S. Bhagwat, Kinase inhibitors for the treatment of inflammatory and autoimmune disorders. *Purinergic Signal* **5**, 107–115 (2009).
66. B. L. Bennett, D. T. Sasaki, B. W. Murray, E. C. O'Leary, S. T. Sakata, W. Xu, J. C. Leisten, A. Motiwala, S. Pierce, Y. Satoh, S. S. Bhagwat, A. M. Manning, D. W. Anderson, SP600125, an anthrapyrazolone inhibitor of Jun N-terminal kinase. *Proc. Natl. Acad. Sci. U.S.A.* **98**, 13681–13686 (2001).
67. A. Urrutia, A. Rubio-Araiz, M. D. Gutierrez-Lopez, A. ElAli, D. M. Hermann, E. O'Shea, M. I. Colado, A study on the effect of JNK inhibitor, SP600125, on the disruption of blood–brain barrier induced by methamphetamine. *Neurobiol. Dis.* **50**, 49–58 (2013).
68. J. Ye, R. Jiang, M. Cui, B. Zhu, L. Sun, Y. Wang, A. Zohaib, Q. Dong, X. Ruan, Y. Song, W. He, H. Chen, S. Cao, Etanercept reduces neuroinflammation and lethality in mouse model of Japanese encephalitis. *J. Infect. Dis.* **210**, 875–889 (2014).
69. M. K. Mishra, A. Basu, Minocycline neuroprotects, reduces microglial activation, inhibits caspase 3 induction, and viral replication following Japanese encephalitis. *J. Neurochem.* **105**, 1582–1595 (2008).
70. S. Das, K. Dutta, K. L. Kumawat, A. Ghoshal, D. Adhya, A. Basu, Abrogated inflammatory response promotes neurogenesis in a murine model of Japanese encephalitis. *PLOS ONE* **6**, e17225 (2011).
71. V. Swarup, J. Ghosh, S. Ghosh, A. Saxena, A. Basu, Antiviral and anti-inflammatory effects of rosmarinic acid in an experimental murine model of Japanese encephalitis. *Antimicrob. Agents Chemother.* **51**, 3367–3370 (2007).
72. Y. H. Ahn, E. S. Ji, J. Y. Lee, K. Cho, J. S. Yoo, Coupling of TiO_2-mediated enrichment and on-bead guanidinoethanethiol labeling for effective phosphopeptide analysis by matrix-assisted laser desorption/ionization mass spectrometry. *Rapid Commun. Mass Spectrom.* **21**, 3987–3994 (2007).
73. Z. Chen, L. Shao, J. Ye, Y. Li, S. Huang, H. Chen, S. Cao, Monoclonal antibodies against NS3 and NS5 proteins of Japanese encephalitis virus. *Hybridoma* **31**, 137–141 (2012).

Acknowledgments: We thank other members of the State Key Laboratory of Agricultural Microbiology for help and fruitful discussions. **Funding:** This work was supported by the National Key Research and Development Program of China (2016YFD05004007), the National Natural Science Foundation of China (31502065 and 31572517), China Postdoctoral Science Foundation (2015M582245), the Special Fund for Agro-scientific Research in the Public Interest (201203082), the 948 project (2011-G24), the Fundamental Research Funds for the Central Universities (2013PY051, 2662016Q003, and 2662015PY083), and the Program of Introducing Talents of Discipline to Universities (B12005). **Author contributions:** J.Y., W.H., and Z.C. performed most of the experiments. H.Z. performed biochemical analysis. B.Z. and D.Z. performed in vivo experiments. J.Y., Y.W., and S.C. planned experiments and analyzed results. J.Y. and U.A. wrote the paper, with contribution from the rest of the authors. S.C., H.C., Z.F.F., and Z.L. conceived and supervised the project. **Competing interests:** The authors declare that they have no competing financial interests. **Data and materials availability:** Proteomic data have been submitted to the Proteomics Identification Database (accession number: PXD004976).

Submitted 21 February 2016
Accepted 15 September 2016
Published 4 October 2016
10.1126/scisignal.aaf5132

Citation: J. Ye, H. Zhang, W. He, B. Zhu, D. Zhou, Z. Chen, U. Ashraf, Y. Wei, Z. Liu, Z. F. Fu, H. Chen, S. Cao, Quantitative phosphoproteomic analysis identifies the critical role of JNK1 in neuroinflammation induced by Japanese encephalitis virus. *Sci. Signal.* **9**, ra98 (2016).

Quantitative phosphoproteomic analysis identifies the critical role of JNK1 in neuroinflammation induced by Japanese encephalitis virus

Jing Ye, Hao Zhang, Wen He, Bibo Zhu, Dengyuan Zhou, Zheng Chen, Usama Ashraf, Yanming Wei, Ziduo Liu, Zhen F. Fu, Huanchun Chen and Shengbo Cao (October 4, 2016)
Science Signaling **9** (448), ra98. [doi: 10.1126/scisignal.aaf5132]

Science Signaling (ISSN 1937-9145) is published weekly, except the last December, by the American Association for the Advancement of Science, 1200 New York Avenue, NW, Washington, DC 20005.